UNIVERSIDAD DE ANTIOQUIA

ZN-C BATTERY WASTE VALORIZATION THROUGH THE MANUFACTURE OF A POLYMERIC MATRIX COMPOSITE MATERIAL

Natalia Cristina Cardona Vivas

Universidad de Antioquia

School of Engineering, Materials Engineering Department

Medellín, Colombia

2020

ZN-C BATTERY WASTE VALORIZATION THROUGH THE MANUFACTURE OF A POLYMERIC MATRIX COMPOSITE MATERIAL

Natalia Cristina Cardona Vivas

Research work submitted as a partial requirement for the degree of:
Master in Materials Engineering

Advisor:
Prof. Henry Alonso Colorado Lopera, PhD

Co-advisor:
Prof. Mauricio Andrés Correa Ochoa, PhD

Line of research:
Composite Materials
Research Group:
Cements, Ceramics and Composites (CCComposites)

Universidad de Antioquia
School of Engineering, Materials Engineering Department
Medellín, Colombia
2020

"As a woman I have no country. As a woman I want no country. As a woman, my country is the whole world."

Virginia Woolf

Acknowledgements

To my parents, especially to my mom, Aurora, for being my support and motivation in all the paths that I have taken in my life. Without her love and understanding, this would have not been possible.

PhD. Henry Alonso Colorado Lopera and PhD. Mauricio Andrés Correa, my advisors of this degree work, for his continuous support and for make it possible the development of this research.

Diego Valle, who not only taught me how to make electrical circuits, but for being there for me at every moment of the development of this research work. Thanks for his patience, motivation and for share with me his knowledge with love.

To the friends of the engineering graduate room for accompanying me with a coffee or a beer and helping me to reduce my stress a little and find solutions in another ways.

The members of the CCComposites group for their collaboration and their words of encouragement.

Abstract

In this research, a comprehensive literature review was conducted over the valorization, use, and circular economy of Zn-C batteries after their useful life. The status of this battery waste in Colombia and Latin America is also presented, as well as some case studies conducted in Medellin involving small business enterprises and research at the university level. The main objective of this work is to develop a polymeric matrix composite material using a conductive resin and battery waste powder comprised of zinc and manganese oxides and carbon, in different proportions as reinforcement, in order to contribute to the environment and innovation of using waste materials as a raw material. This development is complemented with some characterization of raw materials that include scanning electron microscopy, Fourier transform infrared spectroscopy, and x-ray diffraction. Besides, physical, chemical, mechanical, and electrical tests, was conducted in the new material. Results show the high potential of this waste in electronical applications, especially as piezoresistive sensors, showing a good behavior that depends on the amount of battery waste and the electrode configuration of the sensors.

Key words: battery waste, composite materials, conductive resin, characterization, sensors, piezoresistivity.

Resumen

En esta investigación, se realizó una revisión de la literatura sobre la valorización, utilización y economía circular de las baterías de Zn-C después de su vida útil. También se presenta el estado del residuo de baterías en Colombia y América Latina, así como algunos casos de estudio realizados en Medellín que involucran a pequeñas empresas e investigación a nivel universitario. El objetivo principal de este trabajo es desarrollar un material compuesto de matriz polimérica utilizando una resina conductora y polvo de residuos de batería conformado por óxidos de zinc y manganeso y carbón, en diferentes proporciones como refuerzo, con el fin de contribuir al medio ambiente y a la innovación de materiales utilizando residuos como materia prima. Este desarrollo se complementa con la caracterización de las materias primas, incluida la microscopía electrónica de barrido, la espectroscopía infrarroja por transformada de Fourier y la difracción de rayos X. Además, se realizaron pruebas físicas, químicas, mecánicas y eléctricas para el nuevo material compuesto fabricado. Los resultados muestran un alto potencial de este desperdicio para su uso en materiales eléctricos, especialmente como sensores piezoresistivos, mostrando un buen desempeño que depende de la cantidad de residuo de batería y la configuración de la geometría de los electrodos de los sensores.

Palabras clave: residuos de baterías, materiales compuestos, resina conductora, caracterización, sensores, piezoresistividad.

Table of Contents

List of Figures

List of Tables

Chapter 1

1. Introduction

1.1. Problem Statement

A battery is an electrochemical device that can convert chemical energy into electrical energy. It consists of an anode (negative electrode), a cathode (positive electrode), an electrolyte (ionic conductor), separators and an external housing. What differentiates the various batteries, are the materials used as electrodes and electrolytes, which gives each one special characteristics [1]

There are two types of household batteries: single-use or primary, and rechargeable cells or secondary cells.

Table 1. *Classification and use of primary batteries, adapted from [2].*

Battery Type	Components	Characteristics
Primary (Non-rechargeable (Zn / C) or Leclanché type or dry batteries	Manganese Dioxide, graphite, carbon (cathode) Zinc sheet metal (anode) Ammonium Chloride, Zinc chloride (electrolyte)	A low-cost battery. For light applications like flashlights and radios, all types of electrical and electronic equipment simple and low consumption. Called "common batteries".

Battery Type	Components	Characteristics
Magnesium and aluminum batteries	Manganese dioxide with acetylene (cathode) Magnesium alloy, aluminium (anode) Magnesium perchlorate with barium and lithium, chromium chloride (electrolyte)	This battery has two main advantages over the zinc-carbon battery, namely, twice the service life or capacity of the zinc battery of equivalent size and the ability to retain this capacity, during storage, even at elevated temperatures. They are little used for their "voltage delay" and the corrosion of Mg
Zinc / Manganese Dioxide (Zn / MnO_2) or Alkaline	Manganese Dioxide (cathode) Zinc powder (anode) Concentrated caustic, usually Potassium Hydroxide (electrolyte)	They can be used on the same devices as common batteries, but they perform better
Mercury Oxide (Zn / HgO)	Mercury Oxide (cathode) Zinc (anode) Potassium hydroxide, sodium hydroxide (electrolyte)	The zinc /mercuric oxide battery is noted for its high capacity per unit volume, constant voltage output, and good storage characteristics. For hearing aids and medical equipment. Usually button type. They contain about 30% mercury.
Zinc /Air (Zn /O_2)	Oxygen (cathode) Zinc (anode) Alkaline electrolyte	For portable applications. They have a large number of tiny holes in their surface. High capacity. They contain more than 1% of mercury.

Battery Type	Components	Characteristics
Silver oxide	Silver Oxide (cathode) Zinc amalgam (anode) Potassium Hydroxide (electrolyte)	Usually small button type, they contain about 1% of mercury. It is an alternative to mercury oxide.

Among the primary batteries, the most used are zinc-carbon and alkaline-manganese. These batteries usually come in sizes AAA, AA, C, D and 9V [3]. Zn-C batteries have been studied for hundreds of years. The two types of Zn-C batteries most used are those of Leclanché and those of the zinc chloride system. These batteries are characterized by low cost, availability and wide performance in a large number of applications [2]. Alkaline batteries occupy most of the primary battery market: approximately 60%. These are the most economical option that provides great performance at low cost for the operation of various devices [4].

In Colombia, approximately 180 million batteries are used per year, which gives an average of 4 to 6 batteries per person per year. However, this number increases in December, when decorations and toys that require batteries are purchased to its operation [5]. For the year 2019, thanks to "Pilas con el Ambiente" program and its battery waste collection containers located in different parts of the country, a total of 1,680 tons of battery waste did not reach the country's landfills [6]. It is estimated that the useful life of primary batteries is less than one year and that of secondary batteries is 2 to 3 years [7].

80% of the waste from batteries is disposed of in sanitary landfills and 20% goes to landfills and other unsuitable final disposal sites. Based on these data, the company sets out to create stockpiles of batteries and accumulators for selective collection, and then proceed with the reprocessing of the waste materials through recycling or recovery operations [8].

Due to the number of batteries discarded each year, a post-consumption program called Batteries with the Environment was created, where through more than 700 containers arranged in chain stores and various public places, the intention is to collect the batteries that are no longer useful [5].

The most widely used method for recycling primary batteries is using hydrometallurgical processes, through which the metals of the spent batteries are solubilized, testing different leaching agents [9].

With the consumption of batteries, there is a problem regarding their disposal after use, since, when discarded in sanitary landfills, they decrease their useful life, causing different types of contamination due to the chemical reactions generated when these residues are in contact with other substances [10]. For that reason, the objective of this research is to contribute not only to reducing the environmental impact of batteries by finding a potential use of their waste but also to contributes to the innovation of new polymer matrix composite materials for different applications in industry. The residue is a fine powder, from the mechanical processing of used Zn-C batteries, previously obtained in the CCComposites group, from the containers to collect used batteries located within the University of Antioquia, used in other projects of the group, composed of mostly zinc oxide, manganese oxide, and graphite [11].

In chapter 1 introduction and problem statement of this research were presented. Chapter 2 develops the theoretical framework and state of the art. Chapter 3 presents the materials and methods used in this research. Chapter 4 focuses on the composite material manufactured and the characterization. Chapter 5 presents some uses of composites materials in electronical applications and electrical tests in the new material. Finally, chapter 6 presents the conclusions and the future work.

All the above, to face the challenge of the problem of battery waste disposal, to achieve the development of new materials, from different formulations of conductive residue-resin and the study of the new material for potential electronic applications.

1.2. Hypothesis

Develop a polymer matrix composite material using a conductive resin as matrix and Zn-C battery waste powder as reinforcement, mixed in different proportions. Take advantage of the high content of graphite, by providing conductive properties, to give potential use in electrical applications, especially as a piezoresistive sensor.

1.3. Objectives

1.3.1. General objective

- Valorize Zn-C type battery waste, made up of zinc oxide, manganese oxide and graphite, by manufacturing a material made up of ceramic particles with a polymer matrix.

1.3.2. Specific objectives

- Characterize the particles of the battery waste.
- Manufacture different formulations of the battery waste with the conductive resin.
- Carry out a physical-chemical characterization of the samples.
- Determine the electrical conductivity of manufactured samples.

Chapter 2

2. Theoretical Framework and State of Art

2.1. Recycling technologies of Zn-C batteries

2.1.1. Zn-C battery

A zinc-carbon battery is a type of dry cell that offers a potential of 1.5 volts between a zinc metal electrode and a carbon rod through an electrochemical reaction, between zinc and an electrolyte-mediated manganese dioxide. Zinc components work as anode with a negative potential, while the inert carbon rod is the positive cathode. General-purpose batteries can use an aqueous paste of ammonium chloride as an electrolyte, possibly mixed with some solution of zinc chloride [2].

2.1.2. Waste disposal

There are different alternatives for the final disposal of the batteries:

- Landfill: so far, most of the batteries, especially primary batteries, dispositions in municipal waste and sanitary materials [1].
- Stabilization: it represents a previous treatment of the batteries to avoid the contact of the metals with the environment in a landfill. The process is not widely used since it involves high costs [1].
- Incineration: it is used when batteries are disposed in a municipal waste facility and then taken to combustion sites. The incineration of this waste can generate emissions of polluting gases such as mercury, cadmium, lead, and dioxins [1].
- Recycling: the metals present in the batteries can be recycled through hydrometallurgical and pyrometallurgical processes. These recycling processes are being studied in different parts of the world [1].

2.1.3. Waste recovery processes

In recent years, many processes have been developed for battery recycling due to new environmental regulations [9]. Most battery contents can be technically recovered through mechanical and chemical treatments. The recovery of these materials serves to be used in other applications that will be mentioned in the state of the art later..

2.1.3.1. Physical processes

Physical processes are a pretreatment that should be done to battery waste, prior to any other recycling process. The physical processes consist of a sequence of steps: classification, magnetic separation, dismantling, and crushing [12]. The classification is related to a manual process in which Zn-C batteries are separated from the rest of the batteries. In the dismantling stage, it is sought to separate the battery components into their different component materials. Magnetic separation is used to separate the metal from the other materials. Finally, crushing is generally performed using a ball mill, in order to reduce particle size and to obtain powders that improve the efficiency of leaching process. However, crushing is an expensive step due to the energy demand of the process [9].

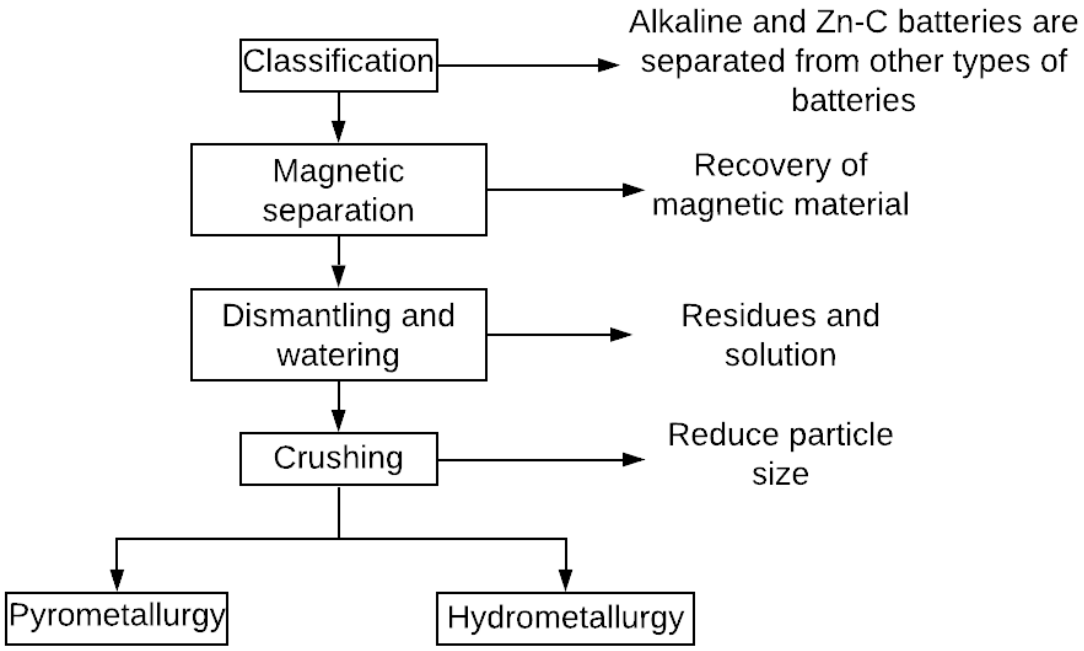

Figure 1. *Mechanical Processing adapted from* [12]

2.1.3.2. Chemical processes

- Pyrometallurgical: They are mainly associated with the production of iron, ferromanganese alloys, among others. Pyrolysis furnaces with a controlled atmosphere are also used in pretreatment to remove mercury and organic material such as plastic and paper. These processes have selective volatilization of metals at high temperatures, followed by their condensation [10]. To obtain zinc and manganese, an oxidation or a smelting furnace is used, where metals are obtained with high purity after certain treatments [13]. The pyrometallurgical route does not require the dismantling stage and is a relatively simple process. Also, through this route, zinc, and mercury can be completely regenerated [12]. The disadvantages of this process are that high energy consumption is required and the emissions of some gases such as dioxins, chlorinated compounds and dusts that require other coupled systems are required to avoid further contamination [14]. There are two possible pyrometallurgical treatments: secondary metallurgy processes that use batteries as raw material, and processes created specifically for batteries (such as pyrolysis, reduction, and incineration) [1].
- Hydrometallurgical: these are processes connected to leaching steps in acidic or alkaline media followed by purification, this in order to dissolve the metal fractions, so the metal solutions that can be used in the chemical industry can be recovered [1].

Hydrometallurgical processes are the most studied to recover metals from battery waste in an efficient way. It is chosen as an extraction process and as an environmental control since the extracted metal will prevent the production of waste. Hydrometallurgical processes consist of the pretreatment steps mentioned above, followed by leaching and separation of metals. Compared to pyrometallurgical processes, hydrometallurgical agents have the advantage of being less expensive and cleaner. Some pretreatment steps are used to improve dissolution rates of the aqueous phase metal [10]. The procedure is long, and the use of different chemicals is required. Wastewater from hydrometallurgical processes can also be a hazardous waste, therefore requiring a separate disposal process. Hydrometallurgical processes have been the most studied for the recycling of Zn-C batteries, for this reason; there are

patented processes since 1984 where zinc oxides and manganese oxides are obtained from battery residues [14].

2.1.4. Available technologies for battery recycling

Several processes have been proposed to recycle the batteries, specially pyrometallurgical and hydrometallurgical in Europe [1]. The most important patented processes that work on industrial scale are Revabat, Batrec, Batenus, Recytec, and Recupyl. Revabat process only treats Zn-C and alkaline batteries; after sorting, the batteries are dismantled and treated with sulphuric acid, from which Mn and Zn are recovered as oxides or salts [15]. The Batrec process (pyrometallurgical) recycles all types of batteries (except Ni-Cd ones). Batteries are pyrolyzed at a temperature of 700 °C and mercury is recovered by distillation. Metallic components are reduced and smelted in the induction furnace at 1500 °C. Fe and Mn remain in the melt and form a ferromanganese alloy, while Zn vaporizes and can be recovered by condensation [16]. The Batenus process handles all types of batteries (except button cells); copper, nickel and cadmium are extracted by ion exchange selectively, while zinc and manganese are isolated by liquid extraction and electrodeposited into two cells to obtain metallic zinc and manganese dioxide [17]. The Recytec process is used specifically for the recycling of battery mixtures. By pyrolysis and magnetic separation, a steel scrap and a zinc dust free from mercury are obtained and sent to the specific recycling processes. Nowadays it is used for the recycling of all types of batteries with the exception of NiCd batteries [18], [19]. In the Recupyl process zinc and manganese are recovered as sulphates [20]. In Table 2 lists different processes for recycling Zn-C batteries, including the most important.

Table 2. *Current technologies of battery recycling*

Name	Process Type	Recover Materials	Reference
BATREC	Pyrometallurgical	Ferromanganese, Hg, and Zn	[16]
U.S. Patent No 5,242,482	Pyrometallurgical	Mercury	[21]
U.S. Patent No 6,009,817	Pyrometallurgical	Products for metallurgical processes	[22]
BATENUS	Hydrometallurgical	MnO2	[17]

Name	Process Type	Recover Materials	Reference
PLACID	Hydrometallurgical	Mercury	[23]
RECYTEC	Hydrometallurgical	Zn, MnO2	[19][24]
HYDROMETAL SPA	Hydrometallurgical	Pb-acid	[25]
REVABAT	Hydrometallurgical	Mn and Zn oxides and salts	[15]
REVATECH			
RECUPYL	Hydrometallurgical	Mn and Zn carbonate	[20]
Acid leaching using sulfuric acid	Hydrometallurgical	Metallic Zn and MnO_2	[26]
U.S. Patent No 5,411,643	Hydrometallurgical	ZnO and MnO	[27]
Integrated process using hydrochloric acid	Hydrometallurgical	Metal mix for use in the steel industry	[28]
Neutral leaching with KOH	Hydrometallurgical	Zn and Mn oxides	[9]
Acidic-reductive leaching	Hydrometallurgical	Zn y Mn sulfates	[29]
Solvent extraction	Liquid-liquid extraction	Manganese	[29]
Chemical Precipitation	Chemical Precipitation	Zn, Mn	[10]

2.1.5. Battery regulations and recycling in Colombia

According to a study by the National Consulting Center and the National Association of Entrepreneurs of Colombia (Andi), about 200 million batteries are sold each year in Colombia but, an estimated 134 million units (67%) of this amount are not recycled [30].

The government has established resolutions for the correct identification of Zn-C batteries [31]. Technical Regulation is applicable to Zn-C and alkaline batteries that are imported or manufactured for their commercialization in Colombia. The technical regulation establishes minimum requirements for labeling, labeling and maximum permissible limits of mercury, cadmium and lead (heavy metals), contained in zinc-carbon and alkaline batteries, in order to protect the country's legitimate objectives of preventing practices that may mislead consumers and protect the environment.

Used batteries are considered as hazardous waste according to the definition and classification found in Decree 4741 of 2005 [32], especially in that indicated in Annex I, that is, they contain zinc, cadmium, mercury, lead, among others.

To mitigate the effect of battery waste, the Ministry of the Environment, Housing, and Territorial Development issue Resolution 1297 of 2010 [33], where the term Extended Producer Responsibility (REP) [34] arises, which forces production and distribution companies to implement an action plan to recover a percentage of the sales of the products that are delivered to the final consumer, guaranteeing a system in which the product can be closed properly.

Resolution 1297 of 2010, "By which the Systems for Selective Collection and Environmental Management of Waste from Batteries and/or Accumulators are established and other provisions are adopted" establishes those producers of 3000 or more units must "formulate, present and implement the Selective Collection Systems and Environmental Management of Waste Piles and/or Accumulators, to prevent and control the degradation of the environment" [33].

Selective Collection Systems (SRS) and post-consumption plans contain the requirements and conditions that producers and importers must meet, to ensure that the elements are properly managed once their useful life has ended, mitigating environmental risk. The SRS in Colombia is born from strategy 4.4 outlined in the National Policy on Hazardous Waste, which sought to promote the management and handling of generated hazardous waste [33].

Post-consumption plans and selective collection systems (SRS) are environmental management instruments focused mainly on the stages of treatment, recycling and final disposal of waste that meet certain characteristics: waste produced by mass consumption activities that have a high generation volume, waste containing dangerous substances of environmental or health interest, even in small concentrations, components with use and/or recovery power, waste with a high environmental or health risk to society, or waste on which consumers have stated a special concern [35].

The post-consumer product return plans are essential for the differentiated management of these since they assign the responsibility of management to the producer, constituting a key piece for environmental control and management by containing the requirements and conditions to ensure the closure of the product life cycle. Post-consumer management begins at the collection points, located in such a way that they do not generate costs or the obligation to purchase a new item, and ends with different use alternatives. Through these collection systems, the aim is to decrease waste and increase the use of solid waste. For example, Duracell, on its website, provides recommendations for the care and use of its batteries. Also, it explains the ingredients of its batteries for the subsequent disposal of waste after fulfilling its useful life. Finally, it not only invites the correct disposal of the waste but also encourages the recycling of battery packaging [36].

The National Authority for Environmental Licenses (ANLA for its Spanish acronym), is the entity that reviews and authorizes the activities subject to environmental licensing, ensuring that they comply with environmental regulations. In Colombia, 33 selective collection systems (SRS) for batteries are in force, to comply with post-consumer regulations [37].

Through Resolution 0308 of 2012, the post-consumer program Recopila was created, presented by the company Tronex S.A.S. as a separate Selective Collection System and Environmental Waste Management [38]. In 2013, its modality became collective, with coverage of 48 municipalities and 71 collection points with the name RECOPILA. Currently, the post-consumption program is made up of 6 importing companies, with geographic coverage of 235 municipalities [39].

In 2016 this post-consumption program had 8,488 containers installed. The battery waste of the containers is collected by the vehicles of Tronex S.A.S., or by the authorized managers then it is taken to the 8 collection centers or the company's warehouses located in Medellín, Bogotá, Barranquilla, Cali, Pereira, Ibagué, Montería, and Bucaramanga. To conclude, the cargo is consolidated and delivered to the managers for their treatment and use [40].

The post-consumer program Pilas Con El Ambiente is the group supported by the House of Appliances of the National Association of Entrepreneurs of Colombia (ANDI), this is a group program made up of the main companies in the battery sector in Colombia. This program began its pilot phase in July 2010 with two points located in Bogotá. Going to 60 points in 2011, and by 2015 it had 3,000 collection points in 29 departments of the country [41]. Today the program brings together the ten biggest battery and accumulator

companies in the country and, it has 4,070 points located in 210 municipalities, for which it has been possible to collect 1,600 tons of household batteries between the years of 2011 and 2019 [42].

In Colombia, there are only methods for the treatment of saline-alkaline batteries with crushing, thermal drying, and grouping of recovered material, which is subsequently sold to other companies.

Ecotec company transforms the used batteries. From the total collected batteries, almost 78% are alkaline and saline batteries, which undergo a process of pyrometallurgy where threads such as crushing and segregation of components such as ferrous metals that serve for national use, the black paste of zinc dioxide and manganese for use abroad, plastic for domestic use, finally slag as cardboard fiber and plastic for final disposal [43].

2.2. Conductive polymers

Conductive polymers are a distinctive group of organic materials that exhibit electrical and optical properties of metals and semiconductors. Polymeric materials can be used in all different areas of electronics [44].

Conductive polymers are classified as materials that exhibit a highly reversible redox behavior and that have the unusual combined properties of metal and plastics [45].

Benzene is the first example of an organic conductive molecule. Although it is not the best conductor, its structure reveals the way in which conductive organic materials behave. In benzene, the carbon atoms are linked to their carbon ring neighbors and hydrogen atoms, alternating single bonds and double bonds, which is known as conjugation. The double and single bonds, are known as π and σ bonds respectively and are a prerequisite for the semiconductor behavior of materials, for this reason, conducting polymers are also known as conjugated polymers, however, not all semiconductor polymers are conjugates [44].

The electronic conjugation between each repeating unit in conductive polymers (CP) provides semiconducting molecular architectures and interesting properties to adapt in detection applications [46].

Currently, there are several investigations of conductive polymers due to their potential in different applications such as biosensors, electrochromic glasses

and screens, antistatic coatings and packaging, solid state batteries, semiconductor electronic devices and membranes [47].

Although there was previous knowledge about conductive polymers, it was not until the late nineties that there was a real understanding of the applications of these materials, this is due to advances in materials science and advanced processing techniques [48].

2.2.1. Conductivity mechanisms

In general, a conductive polymer has a conjugated skeleton formed by alternating single and double carbon bonds (Figure 1). The *p*-orbitals in the series of π bonds overlap each other, allowing the electrons to be delocalized more easily and move freely between the atoms [49].

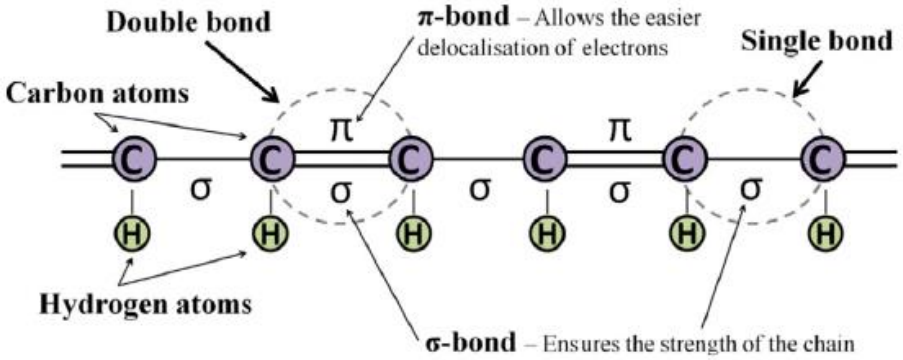

Figure 2. *Simplified diagram of a conjugate spine: a chain that alternates double and simple links* [50]

In addition, different dopants (a negative charge / anion in most cases) can be introduced into the polymers to improve their conductivity [51]. In general, there is a proportional relationship between the amount of dopant used and the conductivity of the doped polymer [52]. The dopant introduces a charge carrier into the system by removing or adding electrons from / to the polymer chain and relocating them as polarons or bipolarons (a localized electron surrounded by a crystal). As an electric potential is applied, the polarons or bipolarons begin to move in the polymer skeleton, allowing the charge to pass through it [53].

According to their molecular size, the dopants can be small and large (chlorides and sodium polystyrenesulfonate, respectively, among others)

[54]. Large dopants are more integrated in the polymer and will not leach over time or with the application of an electrical stimulus, which will give the polymer greater electrochemical stability, while small dopants, on the other hand, can leave and return to enter the polymer with electricity. stimulus [55].

2.2.2. Main conductive polymers

2.2.2.1. Polyaniline

Polyaniline and its related derivatives form a diverse family of conductive polymers in terms of their electronic and structural characteristics. These properties are coupled to the interactions between chains and between chains of subtle molecular level. Amorphous polyaniline (a-NIBP) exhibits a relatively poor inter-chain electron transport behavior, which makes these materials almost one dimension. The crystalline PANI salts (c-PANI), depending on the primary dopant: the presence of water and / or secondary dopant and the processing of samples, can show an improved inter-chain arrangement that results in an increase in the general conductivity [48].

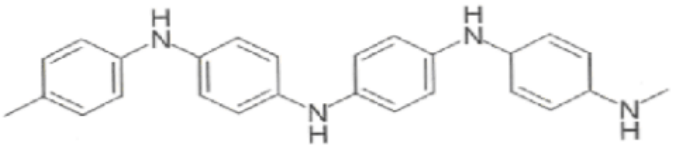

Figure 3. *Basic structure of polyaniline*

2.2.2.2. Poly (phenylene vinyl)

One of the most widely used semiconductor polymers is poly (p-phenylene vinyl) (PPV), which is used in the development of organic LEDs (OLED), due to its electro-optical properties in the neutral state, that is, without doping. The chemical structure of PPV is shown in Figure 4 [44].

PPV occupies a special position in the history of polymer electronics because it was the first to present information regarding electroluminescence [56]. PPV doping has been very effective, achieving conductivities greater than 5 × 103 S cm-1 [44].

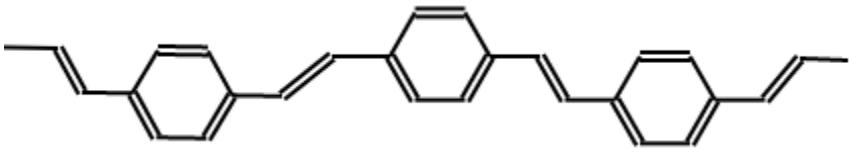

Figure 4. *Basic structure of poly (phenylene vinyl)*

2.2.2.3. Polypyrrole

Polypyrrole is a heterocyclic conductor. It is generally synthesized by chemical or electrochemical means. Chemical synthesis is used when large amounts of material are required and involves mixing a strong oxidizing agent (typically FeCl3) with a monomer solution [57][58]. Electrochemical synthesis is preferred for research purposes because of the simplicity of the technique, control of material thickness, geometry and location, ease of doping during synthesis, wide selection of available doping ions, and generation of good quality films [59], [60]. It leads to the development of conformity deposits of the adherent surface, that is, thin solid films, from the mass solution phase of the monomer units. Electrodeposition on the positively polarized working electrode is performed through a condensation reaction between the monomer units of the five-membered pyrrole heterocycle.

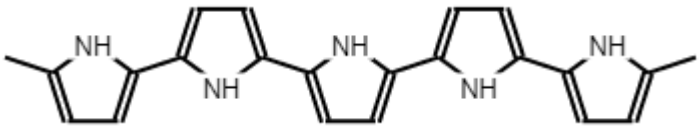

Figure 5. *Basic structure of polypyrrole*

2.2.2.4. Polyacetylene

They are a group of organic compounds with alternating single and double covalent bonds. It is known as the prototypic conjugate polymer due to its structural simplicity [61]. Polyacetylenes are distinguished from other organic chains by their rigidity, which makes them viable for molecular nanotechnology [60]. Polyacetylene does not show a metallic behavior, but thanks to its bandgap, it behaves like a semiconductor, for this reason, it has a high electrical conductivity generated by the delocalization of π bonds [44].

Polyacetylene is still the subject of much research, as it has difficulties regarding its processing and stability and the possible commercial uses of the product. These problems are being addressed from the copolymers in the synthesis of the polyacetylene chain, as well as from the catalysts used and the different conditions of temperature and pressure in the polymerization process [61].

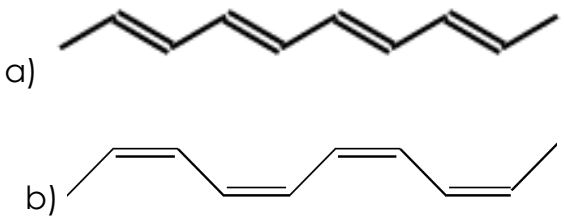

Figure 6. *Structure of a) trans-polyacetylene y b) cis-polyacetylene*

2.2.2.5. Polythiophene

Polythiophene is a conductive polymer that shares certain optical properties with PPV, they are electroluminescent. The optical properties of polythiophene are interesting as polymer turns blue compared to undoped polymers, which is red. The level of doping governs the color of the Polymer [44].

Polythiophene is a polymer of interest because it offers many possible routes for its synthesis. It has good environmental stability in a neutral and doped state and may be subject to reversible redox change. (The ability to reduce and then oxidize the polymer is useful in applications where change can be useful, such as in electrochromic devices, where the redox reaction changes optical properties such as transparency or color) [44].

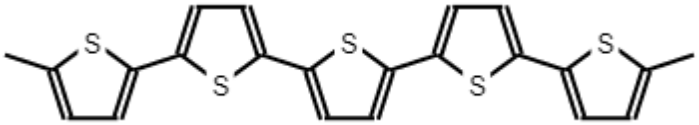

Figure 7. *Basic structure of polythiophene*

2.2.3. Some applications of CP

Recent studies refer to a new group of advanced composite materials, known as CP nanocomposites, combining flexibility and conductivity and

with the advantages of nanofiller that can have applications in different devices [62].

CP, due to their multifunctionality, ease of synthesis and stability, have been used together with other commercial hydrophilic sorbents for the extraction of polar compounds, although they have a smaller specific surface area, better interactions are obtained with this type of compound [45].

The CP have been functionalized to obtain a better performance as sensors, since through intelligent structural modifications, detection capabilities can be granted, so that they can overcome the basic function at molecular levels, such as the recognition and control of processes chemicals, as well as reporting chemical and electrochemical properties, effectively improving the selectivity and detection of an analyte and the performance of the sensor in general [46].

The functionalization of silicon nanowires with CP grafts has been carried out to improve conductivity and understand the fundamental properties when working at the nanoscale, as well as their application in devices such as field-effect transistors, chemical or biological sensors, battery electrodes and photovoltaic [63].

CP have been used in biomedical applications for the manufacture of artificial muscles, controlled drug release, neuronal recording, stimulation of nerve regeneration, among others. Furthermore, electrically active tissues, such as the brain, heart, and skeletal muscle, provide the opportunity to couple electronic devices and computers with human or animal tissues to create therapeutic body-machine interfaces [53].

Due to the excellent electronic, optical, and mechanical properties, high structural stabilities, easy processing, and economic synthesis costs, CP and their derivatives, nanocomposite conductive polymers, are widely used in various optoelectronic devices, which are devices that involve light, either its use or generation. Light sensitive devices function as optical transducers or electrical devices that include solar cells, photodiodes, and phototransistors. Light-generating devices can be light-emitting diodes (LEDs), laser diodes, and cathode-ray tubes [62].

In addition to light-emitting diodes, CP are being used for the production of organic light-emitting diodes (OLEDs), which are a type of LED in which light is emitted by a layer of organic materials in response to a current electric. In other words, the electroluminescent layer is a film of organic materials. Currently, OLEDs are used more frequently for displays and lighting since compared to LCDs, they consume less energy, provide better image quality, have a shorter response time and a wider viewing angle, in addition to allowing the manufacture of ultra-thin devices and flexible displays [64].

CP can be created to be biocompatible and biodegradable. Its physical properties can be easily optimized for a specific application through the binding of biologically important molecules in the polymer using one of the many available methods for its functionalization. Their conductive nature allows the cells or tissue grown on them to be stimulated, the physical properties of polymers are influenced after synthesis, and the drugs bound to them are released, by applying an electrical signal [52].

CP can become efficient thermoelectric generators by summarizing various architectural designs previously reported. These devices have tremendous potential to harness low-temperature heat (for example, body/appliance heat, geothermal/ocean heat, etc.) to power portable medical sensors and smart electronic devices, so CP can potentially be used in the thermoelectric industry, with low costs and high functionality [65].

Conductive polymeric membranes have been developed for scale prevention in water treatment and desalination. Electrically, the conductive properties of membranes suggest a wide range of possible advantages and applications including the development of scale resistant biomembranes, scale control, and an electrochemical system combined with membrane processes for water treatment and desalination [50].

CP are high-tech materials with high energy efficiency, bright colors, and superior environmentally friendly optical properties. For this reason, it is possible to obtain electrochromic properties using new multifunctional monomers in the polymerization of thiophene groups to obtain a more stable material that has better optical properties [66].

2.3. Composite Materials in Electronic Applications

2.3.1. Composite materials

Composite materials are a multiphase material that is artificially made. They are made up of reinforcing material and matrix. During the composite molding process, the matrix material undergoes a series of the complex processes to form a whole body with determined shape. The constituent phases must be chemically dissimilar and separated by a distinct interface. The properties of composites are a function of the properties of the constituent phases, their relative amounts, and the geometry of the dispersed phase [67].

Composites can be classified in terms of matrix phases: ceramic-based composites (CMC), polymer-based composites (PMC), and metal-based composites (MMC). Metals or polymers are commonly used as a matrix material. In ceramic composites, the reinforcement is chosen to improve the fracture toughness. A most important factor in choosing the matrix and reinforcement is the resultant bond strength and combined physical properties [68].

2.3.2. Polymeric matrix composite materials

Polymer-matrix composites (PMCs) consist of polymer resin (denotes a high-molecular-weight reinforcing plastic) as the matrix, with fibers or particles as the reinforcement medium. These materials are used in a diversity of composite applications, due to ease of fabrication, and cost [69].

The prominent advantages of polymer matrix composite materials are their high specific strength and high specific modulus. The specific strength is the ratio of strength and density and the specific modulus is the ratio of modulus and density, and the dimensions or units are both lengths. They also have good damping characteristics. Besides, polymeric matrix composites have superior electric insulation performance, high frequency dielectric properties, good friction behavior, excellent chemical corrosion resistance, special optical, electrical and magnetic properties that depends on the configuration between the matrix and the reinforcement and if the reinforcement is a fiber or a particle [69].

2.3.3. Piezoresistive sensor with polymeric matrix composites

Polymers are widely being used as strain sensors, chemical sensors, biosensors, robotic arms, prosthetic limbs, energy devices and power sources in all domain of science and engineering [70]. Traditional metal foil sensors do not have sufficient flexibility for biomechanical and other applications. Piezoresistive polymer composites are an exciting new technology for filling the need for versatile yet mechanically strong properties [71]. Furthermore, polymeric matrix composite materials have characteristics such as flexibility and stretchability, which makes them a significant option for the develop of sensors such as motion detectors and wearable devices that require little thickness and high sensitivity [72]–[75].

2.4. State of Art

The recycling of batteries containing cadmium and zinc can be done from their leachate using an extractant called Cyphos IL 104 diluted in toluene and synthesis of zinc and cadmium oxides from the charged organic phases, thus obtaining a quantitative recovery of more 90% high purity Cd and Zn [76].

Fine particles of zinc and manganese oxide can also be obtained by pyrolysis between 850º and 950ºC of alkaline and Zn-C batteries [77].

Besides, acid and alkaline leaching studies have been carried out for the recovery of Mn and Zn from spent alkaline batteries, using hydrochloric acid as a solvent under the appropriate conditions of concentration and temperature, resulting in the separation and recovery of the two components [78].

Recent studies show that the recovery of metals such as Cd in battery waste is also possible, through the chitosan polymer that has an affinity for metals [79].

Carbon rods from Zn-C battery waste have been used to obtain CdS and TiO2 films. To obtain the film, it was carried out using a chemical deposition bath with surfactant molecules as a binding agent to promote the union between the semiconductor film and the substrate. Subsequently, an evaluation of the photocatalytic activity of CdS / C and TiO2 / C in hydrogen

production was carried out, obtaining positive results with both catalysts, especially with CdS / C [80].

Considering the low cost of obtaining carbon and manganese from battery waste, a porous biocomposite was synthesized for the adsorption of Pb (II) from wastewater. This biocomposite was made by co-pyrolyzing the battery waste with sawdust [81].

Zn and Mn oxides are obtained from battery waste, to later synthesize Mn-Zn ferrite through a hydrothermal process, using in turn solution of ferrous chloride waste from iron plants or recycled electronic plants as raw materials for departure [82].

A study was conducted to obtain Mn-Zn magnetic ferrite nanocrystals from Zn-C battery waste using the sol-gel citrate self-combustion method [12].

Solid MnOx and ZnMnO catalysts can be obtained through biohydrometallurgical processes from battery waste to be used in the combustion of volatile organic compounds, obtaining complete conversions of these compounds and high selectivity to CO2 [83].

Manganese oxides were obtained from Zn-C battery waste using a biohydrometallurgical process to use the oxides as catalysts for the oxidation of volatile organic compounds, comparing their activity with that of the oxides obtained in the laboratory, showing good performance for the elimination of said compounds [83].

It is possible through the recycling of batteries and electronic waste, the recovery of nanomaterials that are conducive to industrial-scale operations [84].

It is possible to integrate a polymer, specifically the OSTEMER, to a PCB to include channels through a microfluidized method with dry glue, obtaining a homogeneous interface, free of voids and a PCB resistant to compression and ready for the respective electrical characterization [85].

PLA associated with graphene was used for printing electronic circuit elements as conductive material and PLA Hatchbox as a dielectric material, setting as a reference the use of this manufacturing technique to obtain said elements using new materials [86].

Recent studies refer to a new group of advanced composite materials, known as nanocomposite conductive polymers, combining flexibility and conductivity and with the advantages of nanofillers that can be applied in different devices [62].

Conductive polymers, due to their multifunctionality, ease of synthesis and stability, have been used together with other commercial hydrophilic sorbents for the extraction of polar compounds, although they have a lower specific surface, better interactions are obtained with this type of compounds [45].

Conductive polymers have been functionalized to obtain better performance as sensors, since, through intelligent structural modifications, detection capabilities can be given to polymers, so that they can overcome the basic function at molecular levels, such as recognition and chemical process control cos, as well as reporting chemical and electrochemical properties, effectively improving the selectivity and detection of an analyte and overall sensor performance [46].

The functionalization of silicon nanowires with conductive polymer grafts has been carried out to improve conductivity and understand the fundamental properties when working at the nanoscale, as well as its application in devices such as field-effect transistors, chemical or biological sensors, electrodes of batteries and photovoltaics [63].

Owing to their exceptional mechanical, electrical, and thermal properties, carbon nanotubes (CNTs) have attracted considerable interest. This combination of properties and special morphology (high aspect ratio, nano-size diameter) makes CNTs potentially ideal candidates as a filler for polymer composites with improved mechanical properties, electrical conductivity and multifunctionality. A new manufacturing method has been introduced to disperse CNTs and carbonyl iron powders (CIP) in polymeric composites efficiently and uniformly. Different specific proportions of CNT and CIP were explored for the electrical and piezoresistive detection of the compounds. Incorporation of CIP into CNT-embedded polymeric compounds was shown to improve piezoresistive detection characteristics under cyclic tensile strain loads [71].

The influence of the polymeric matrix on the mechanical and electromechanical properties of polymeric composites prepared by solvent casting has been studied, using CNTs as fillers. Poly(vinylidene fluoride), styrene-b-(ethylene-co-butylene)-b-styrene and thermoplastic polyurethane have been successfully used as pressure sensing materials for human walking detection, with an electronic circuit developed to measure and compare different polymer and composite materials. All composites can make sense of the human walking movement [87].

This paper reports on the piezoresistive response of carbon nanotube/poly(vinylidene fluoride), CNT/PVDF, composites prepared with different CNT types with and without functionalization, via in situ-generated diazonium compounds. Thus, a close relationship between the threshold of percolation and the piezoresistive response was demonstrated. The electromechanical response, as defined by the gage factor, reaches values of up to 3.9, is among the largest obtained for thermoplastic composites and demonstrates the suitability of these materials for sensor applications [88].

The mechanical properties, electrical conductivity and piezoresistive response of thermosetting polymer nanocomposites comprising carbon nanotubes (CNTs) with different topologies. CNTs and graphene contribute to the improvement of the mechanical properties of the sensors, because they have a higher aspect ratio, a greater number of pendant links and functionalities and a greater specific surface area of their fillers. The increased piezoresistive sensitivity is explained in terms of their higher excluded volume within the composite [89].

This paper explored the effect of CNT agglomeration on CNT-polymer composite piezoresistivity. Results show that the CNT agglomeration is responsible for reduced electrical conductivity and piezoresistivity nonlinearity with respect to zero strain. The current work provides a useful analytical tool for the design of smart sensing and multifunctional polymer composites [90].

Poly (4-styrenesulfonic acid) (PSSA) and Carbon Nanofiber (CNF) solution was mixed in polyvinylidene fluoride (PVDF) polymer matrix to prepare PVDF/PSSA/CNF blend membrane sequence. e The results show

improvement of the gauge factor and piezoresistive sensitivity in the presence of PSSA, with increasing concentration of CNF [91].

Considering thermoplastic polyurethane (TPU) and/or olefin block copolymer (OBC) as polymer matrix and carbon black (CB) as conductive filler, a sensor was developed by a design of the formulation variables of extrusion-based manufacturing. Highly loaded binary and ternary composites with CB2 exhibit a more obvious strain-dependent dynamic hysteretic behavior as they switch from a dual peak to a single peak pattern towards the sensing strain limit, which is interesting for self-diagnosis [92].

Conductive polymer composites are prepared as filler with a matrix of polyvinylidene fluoride (PVDF) and Multiwalled carbon nanotube (MWCNT). In the composite, an optimal combination of ductility and piezoresistivity is found slightly above the threshold of electrical percolation, showing a maximum fracture strain approximately 4 times higher than the pure PVDF samples, as well as an outstanding piezoresistive response sensitivity [93].

A porous foam sensor based on carbon black/polydimethylsiloxane (CB/PDMS) is proposed to be fabricated. Here, the large linear sensing range is primarily related to the nice CB conductive network on the cross-linked PDMS foam and the composite material 's high modulus and elasticity, which ensures the homogeneous deformation of the foam under compression. The CB/PDMS foam is then assembled as a wearable sensor and displays a good ability to monitor human body motions, such as finger and elbow bending, walking, jumping, and squatting, etc. The porous foam sensor also has a good ability to separate oil/water which shows a multifunctional feature [94].

Chapter 3

3. Materials and Methodology

3.1. Materials

Battery waste powder was previously obtained from a local provider at Medellín using grinding of alkaline and Zn-C. The grinding process gave a black ceramic powder, plastic, carbon, paper, and steel. Plastic, paper and steel were initially manually removed. Then, a sieve (U.S. Standard Sieve 30) was used to remove bigger particles. The particle size of the waste resulted after grinding batteries was 0.2 µm. The final waste used, is a black powdered mix, mainly composed of ZnO, MnO_2 and graphite particles [11].

The conductive polymer is a styrene vinyl acrylic resin with carbon particles obtained from Voltec Electrónica, Colombia. These resins have better technical performance than traditional vinyl acrylic resins. Coatings developed with this type of resins have greater resistance to fouling, less water absorption, greater resistance to the alkalinity of cement, greater resistance to ultraviolet rays and greater resistance to saponification of the wall, properties that make the coating have longer lifespan. the carbon particles in the resin give it its conductive character, for this reason, this resin can be used as a contact medium to correct electrical circuits without the need for wiring, obtaining a durable finish.

3.2. Methodology

3.2.1. Fabrication of composite material

Five different solid weights fraction contents were explored: 0, 5, 10, 15, and 20wt% of battery waste (BW). The mixing of materials was conducted manually for few minutes. An aluminum mold of 12 mm in diameter and 4 mm in height was used to prepare samples for characterization, hardness,

and piezoresistivity tests. To compression test, samples were fabricated in a PVC mold maintaining the recommended ratio for compression specimens of ASTM D695. The samples were left at room temperature for about 72 hours for the pure resin sample, and 48 hours for the waste-resin mixtures, until they hardened completely. The samples of 0wt% were fabricated in an aluminum mold of 9 mm in diameter and 20 mm in height. The experimental design is shown in Table 3.

Table 3. *Design of experiments composite material*

Sample	Resin (%wt)	Waste (%wt)
1	100	0
2	95	5
3	90	10
4	85	15
5	80	20

3.2.2. Characterization of composite material

When the specimens dried completely, their dimension of radius and height was obtained using a Vernier caliper. For density and dimension stability tests, five specimens were fabricated using different amounts of resin and battery waste. Density was determined by the dimensional method, in which measurements of height and diameter of the specimens were taken. A high precision Mettler Toledo balance was used to weight the specimens.

Scanning electron microscopy (SEM) and energy dispersive spectroscopy (EDS) were used to analyze the specimens in a JEOL JSM 6700R microscope operated in high vacuum mode. Specimens were cryogenized and then mounted on carbon tape and gold sputtered with a Hummer 6.2 apparatus at 15 mA AC for 30 sec to obtain a thin gold film. X-ray diffraction (XRD) characterization was conducted in an X'Pert PRO diffractometer (Cu Ka radiation, λ=1.5406 Å), using a 45 kV voltage and scanning angle 2θ between 10 and 90°.

Shore D hardness was measured using a CEAST hardness tester for shore D. The test consists of placing the durometer needle in the sample and pressing until this was fully inserted. Then, the displacement in the durometer scale was recorded. Compression tests were conducted on the fabricated specimens using a Shimadzu AG250KN universal testing machine following the recommendations of ASTM D695 at 1.3mm/min crosshead speed. Compressive strength was calculated from the stress-strain compressive curves.

Fourier Transformed Infrared spectroscopy (FTIR) analysis was performed in a Perkin Elmer Spectrum UATR Two Spectrometer, from 4000-500 cm^{-1}, with 64 scans and a resolution of 1 cm^{-1}.

3.2.3. Piezoresistive tests

Sensors were manufactured using three different geometries for the electrodes (see Figure 8a) to assess their piezoresistivity. The electrode geometries were designed in the Eagle software and then printed on bakelites. Circuits were constructed using the electrodes with specimens 5, 10, 15, and 20% of battery residue (see Figure 8b). Finally, compression tests were performed using a Shimadzu AG250KN universal testing machine (see Figure 8c). One test evaluated dynamic response over a range of forces. The universal testing system was programmed to increase the force of monoaxial load cells from 0 to 500N at a rate of 10 N / s. The machine kept the force for 5 seconds as soon as the force reached 500N, and then started to reduce the force at the same pace. Stored force and voltage every 500ms [101]. The acquisition system used 16 bits analog to a digital converter to take voltage variations from the resistance divider circuit at a sample frequency of 200Hz. Additionally, the acquisition system acquired force data through sample period from the universal test machine. A program was also developed to monitor changes in the voltage in real time as force increased with Arduino. Electrical tests were performed at room temperature.

a)

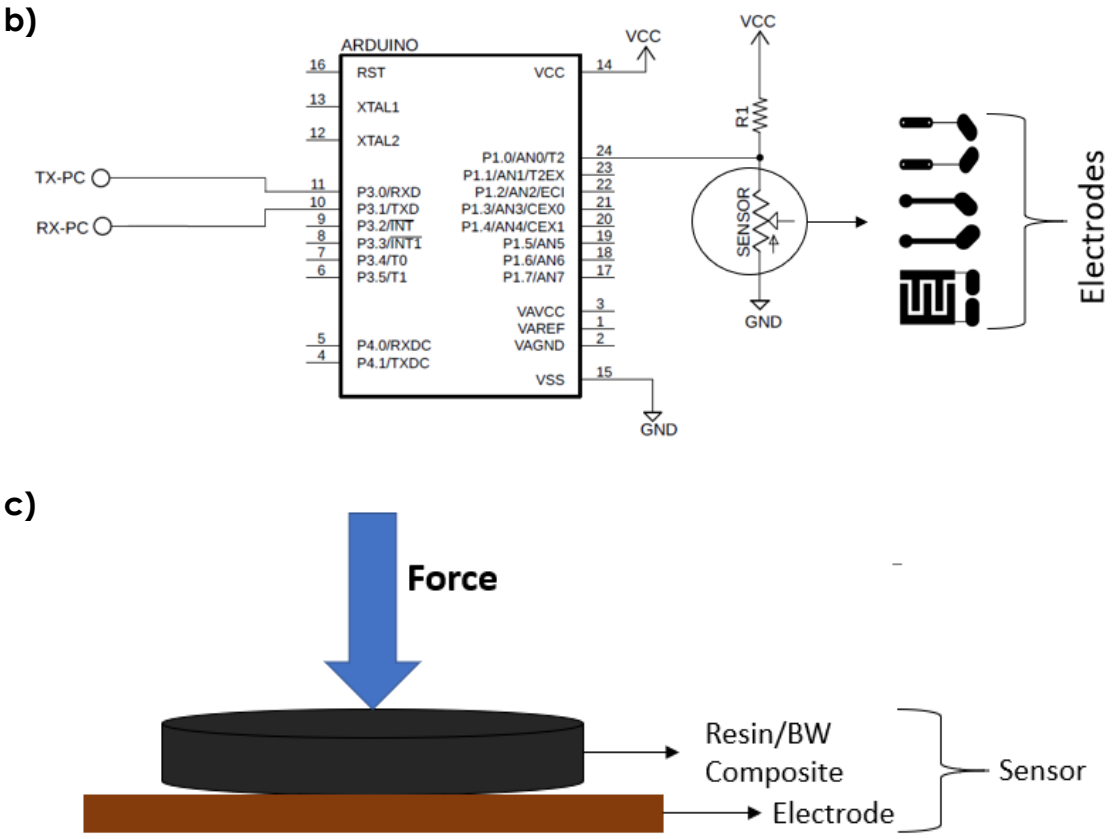

Figure 8. a) *Electrode configuration* ***b)*** *Fabrication of sensor using different geometries* ***c)*** *Mounting on the universal machine to evaluate piezoresistivity*

Chapter 4

4. Raw Materials Characterization

4.1. Characterization of battery waste

Battery waste powder was analyzed by scanning electron microscopy (SEM). Although, a quantitative analysis was also carried out with energy dispersed spectroscopy (EDS). All samples after the drying process were mounted on a carbon tape and gold sputtered with a Hummer 6.2 system, at conditions of 15 mA AC for 30 sec, to make a thin film of Au of about 1nm. The SEM used was a JEOL JSM 6700R in a high vacuum mode.

The crystal structure was identified by X-ray diffraction (XRD) characterization, conducted in an X'Pert PRO diffractometer (Cu Ka radiation, λ=1.5406 Å), using a 45 kV voltage and scanning angle 2θ between 10 and 90º.

4.1.1. Results Scanning Electron Microscopy

From Figure 9 related to micrograph of battery waste powder, it is obvious a highly irregular microstructure with amorphous grains. Although in Figure 10 is observed that the average particle size is 0.19 μm, from the SEM image (see Figure 9) there are smaller particles in the nanometric order. EDS analysis shows that the peaks of Zn, Mn, O, and Cl are predominantly high in the spent battery powder. Presence of C peak can be attributed to the trace of carbon from carbon rod while dismantling and/or from carbon tape in the battery waste. Al and Fe can be observed too (see Table 4).

Table 4. *Composition of battery waste obtained by EDS*

	Element	C	Zn	Mn	O	Fe	Al	Cl	Total
Battery waste	(weight %)	44.67	14.76	21.90	10.36	1.05	0.48	6.79	100

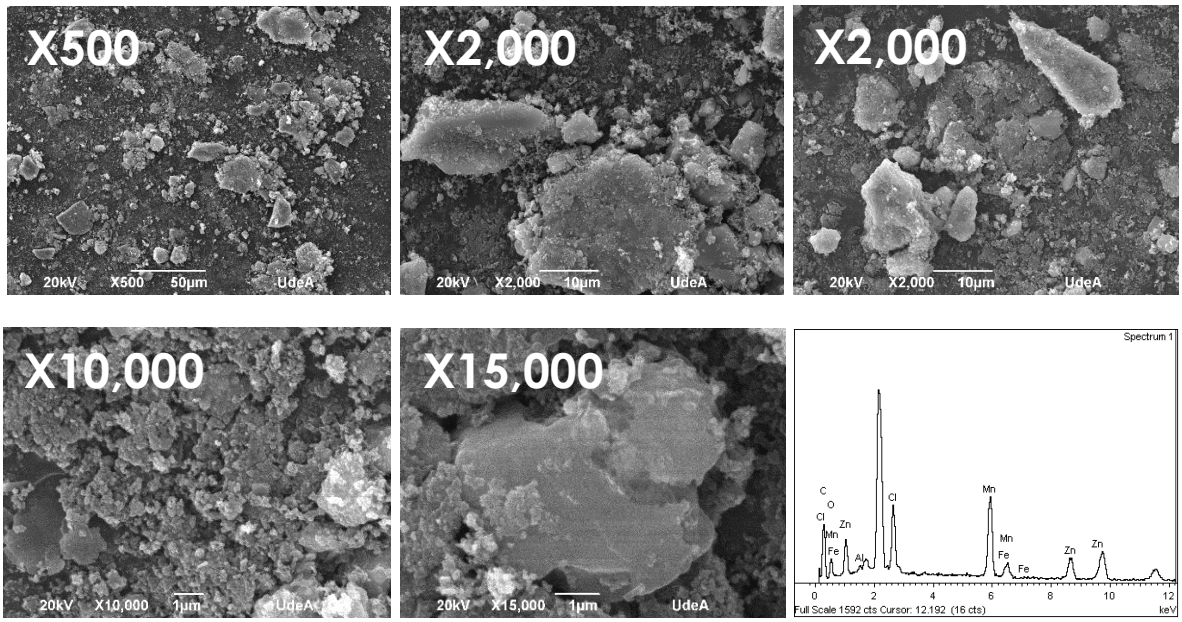

Figure 9. *SEM-EDS analysis of battery waste*

Figure 10 is observed that the battery powder has a uniform particle size distribution, and the average size is 0.19 µm.

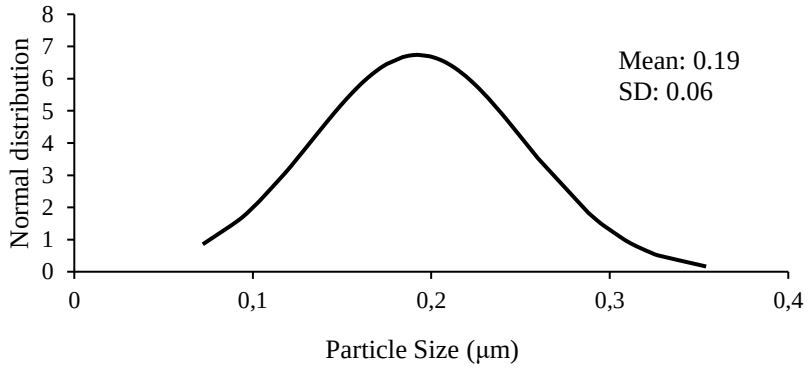

Figure 10. *Particle size distribution of battery waste*

4.1.2. Results of XRD

Figure 11 shows the XRD spectra for the Zn-C BW. It indicates that the battery waste is composed of graphite (C), zincite (ZnO), simonkolleite ($Zn_5(OH)_8Cl_2 \cdot H_2O$), hetaerolite ($ZnMn_2O_4$) and sylvite (KCl). Due to the presence of $ZnCl_2$ as an electrolyte, simonkolleite is possibly formed during battery discharge [13]. K is derived from electrolyte, which is potassium hydroxide. Other XRDs of this residue have been reported in papers, in which

ZnMn2O4 appeared as a common phase [77], [95], [96]. The existence of these crystalline phases suggests that the main elements in the battery waste are Zn, Mn, Cl and O, which is consistent with the EDS report (see Figure 9).

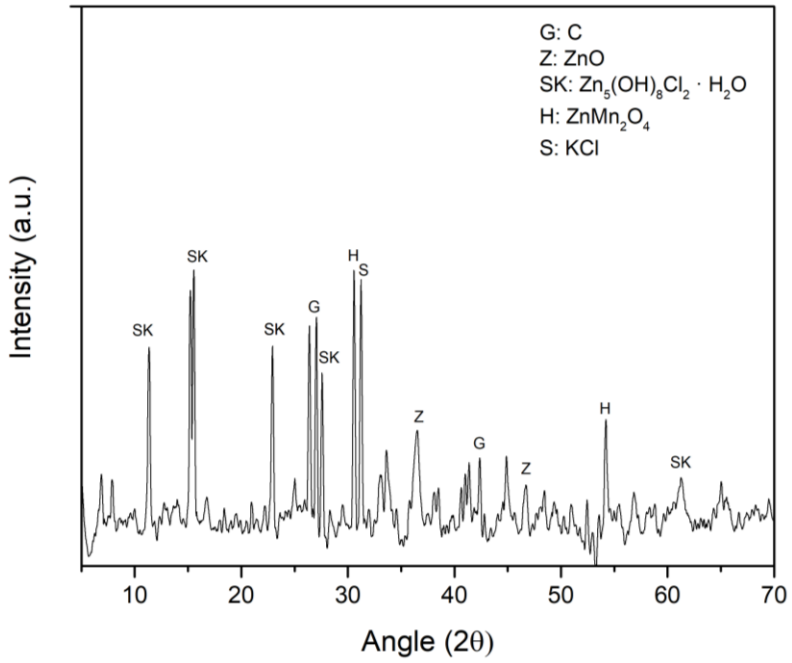

Figure 11. *XRD for the primary battery waste from Colombia used in this research*

4.2. Characterization of conductive resin

Conductive resin was analyzed by scanning electron microscopy (SEM). Although, a quantitative analysis was also carried out with energy dispersed spectroscopy (EDS). At the same conditions and using the same instruments that the battery waste characterization.

4.2.1. Results Scanning Electron Microscopy and Electron Dispersive Spectroscopy

Figure 12 is related to SEM image for sample of conductive resin shows slabs oriented in the zone of the cryofracture. Also, an amorphous matrix can be identified, corresponding to the diffuse or smooth zones. The reinforcement can be observed in the oriented slabs related to the carbon particles present in the sample.

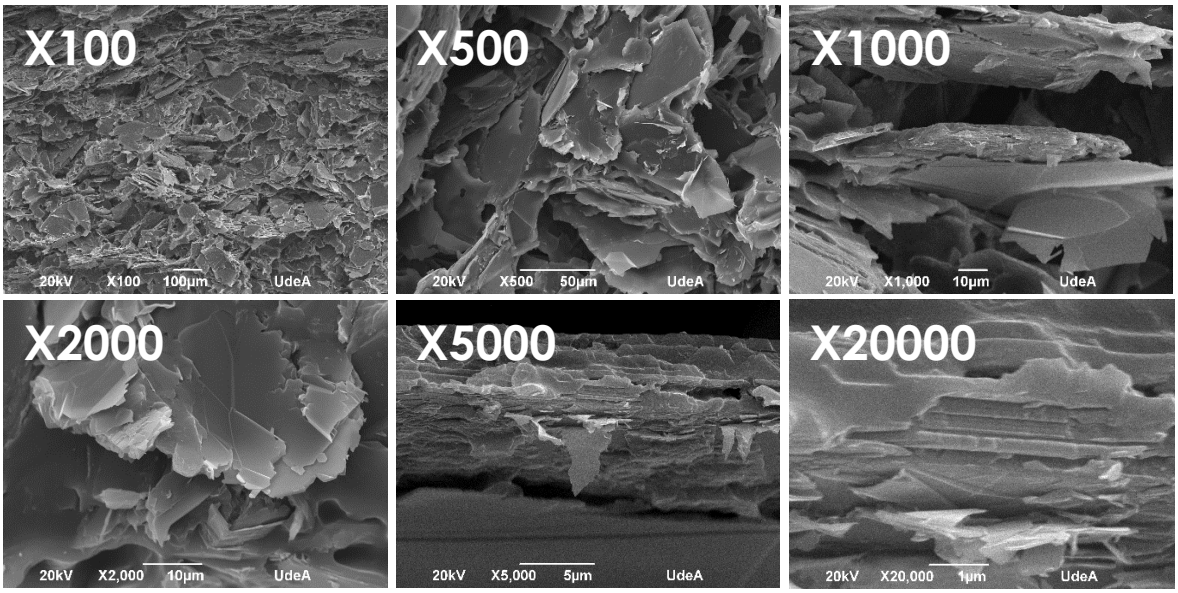

Figure 12. *SEM micrograph of conductive resin*

Figure 13 shows the size distribution of plates corresponding to carbon in the resin (the plate size was 69.9 µm).

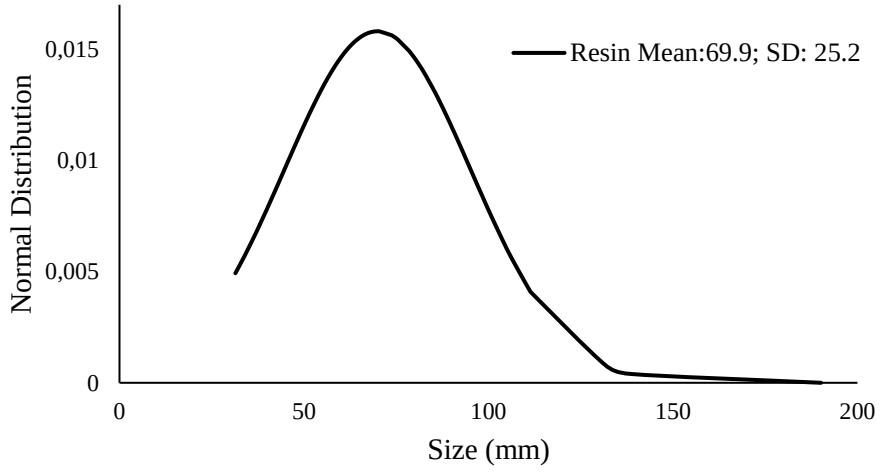

Figure 13. *Distribution of resin plate size*

In the EDS mapping (see Figure 14) the distribution to a greater extent of elements such as carbon and oxygen is observed, which are the constituents of the resin; and to a lesser extent elements such as iron, silicon and aluminum that help it the conductive character. Table 5 confirms the elements present in the conductive resin.

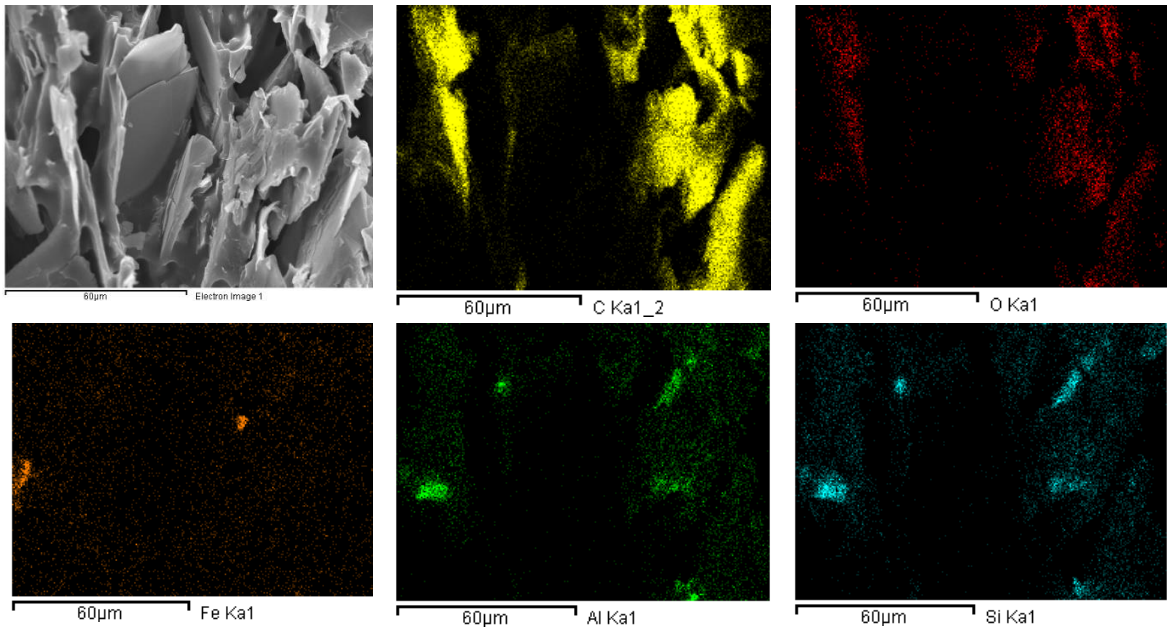

Figure 14. *EDS Mapping of conductive resin*

Table 5. *Composition of resin obtained by EDS*

	Element	C	O	Fe	Al	Si	Total
Resin	(weight %)	83.83	11.62	2.30	1.01	1.24	100

4.3. FTIR battery waste and conductive resin

Figure 15 shows the FTIR spectrum for resin, and battery waste. The black color of the specimens makes detection in the infrared equipment challenging. The spectrum of resin shows a peak close to 3000 cm-1 which is the characteristic peak of acrylic resins. EDS in Figure 14 is the most suitable method of quantifying the chemical composition of the compound.

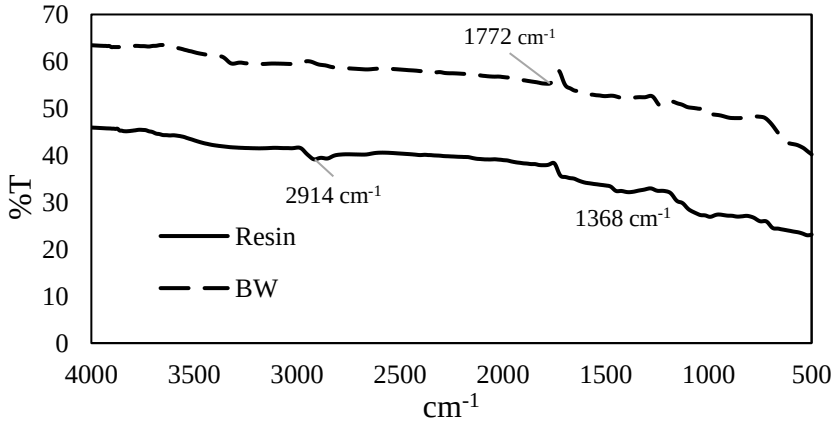

Figure 15. *FTIR for resin and battery waste*

Chapter 5

5. Manufacture and Characterization of Composite Material

5.1. Dimensional stability

The initial and final volume was calculated using the parameters of the cylinder with height (h), and radius (r), then, volume (V) is calculated as V = π * r2 * h. Equation 1 was used to determine the percentage of contraction of the specimens. For the specimen with 0wt% the contraction was 68.37%. For the 5, 10, 15, and 20wt% BW specimens the contraction was 15.97%. Taking into account the dimensions of the mold and from Figure 2a, a high percentage of contraction is observed for the sample with 0wt% BW. Dimension changes observed are lower in the other specimens, which is expected as the waste composition has ceramic powders, therefore, is expected an increase not only thermal but also dimension stability, see Figure 2b. The sample with 0wt% BW exhibited the highest dimensional changes, see Figure 2a.

$$\%Contraction = \frac{V_0 - V_f}{V_0} * 100 \quad (1)$$

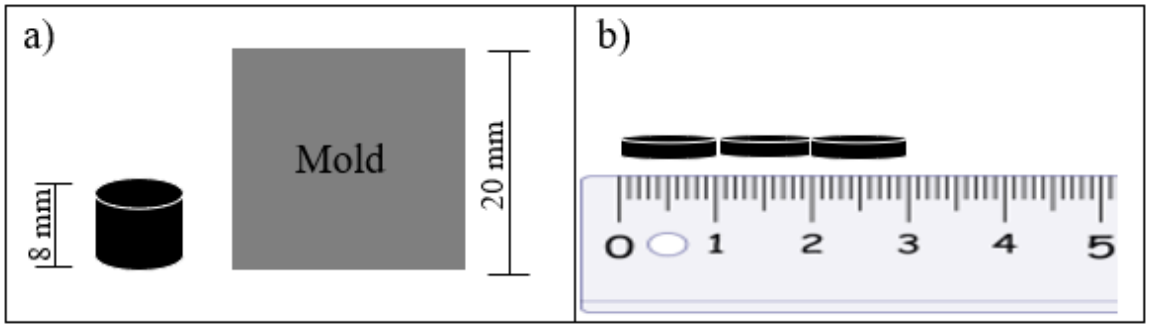

Figure 16. a) *Dimensional change in the resin specimens.* ***b)*** *Composite specimens*

5.2. Chemical characterization

5.2.1. SEM Results

In some areas, the battery waste is more concentrated, even agglomerated, which can be seen in Figure 17 which is the specimen with 5 wt% of BW. The agglomeration can be explained by the difficulty in the mixing process, which generates a poor dispersion of the residue in the mix. Carbon particles appeared, mostly, as imbibed particles in the matrix.

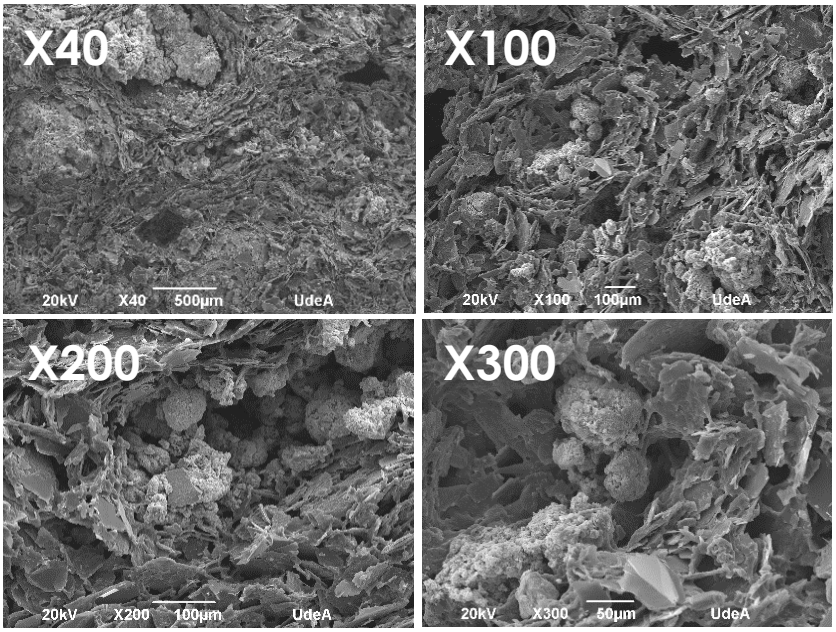

Figure 17. *SEM micrograph of specimen 5wt% BW*

Table 6 shows the percentage of the elements present in the specimen 5wt%BW. In the EDS mapping (see Figure 18) the distribution to a greater extent of elements such as carbon and oxygen is observed, which are the constituents of the resin and the high content of graphite in the battery waste; and to a lesser extent elements such as aluminum, chlorine, iron, zinc, manganese and silicon. These elements are relative to the other compounds of battery waste, specially, manganese and zinc.

Table 6. *Composition of specimen 5wt% BW obtained by EDS*

	Element	C	O	Al	Si	Cl	Mn	Fe	Zn	Total
5wt%BW	(weight %)	70.63	11.90	0.76	1.02	3.35	5.28	1.41	5.65	100

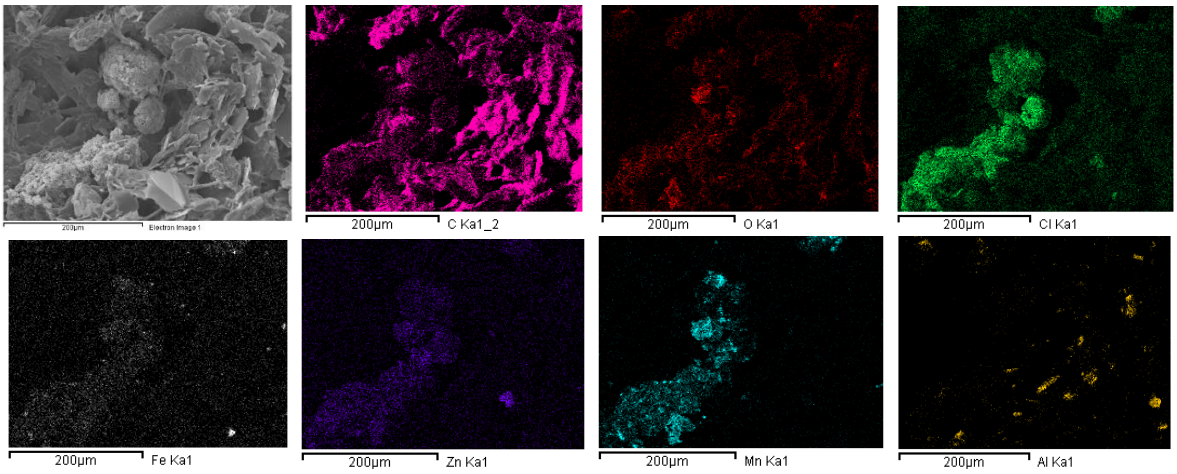

Figure 18. *EDS Mapping of specimen 5wt% BW*

Figure 19 which is the specimen with 10wt% of BW, shows a greater agglomeration of particles because there is a greater concentration of residue in the sample. The smooth parts correspond to the resin.

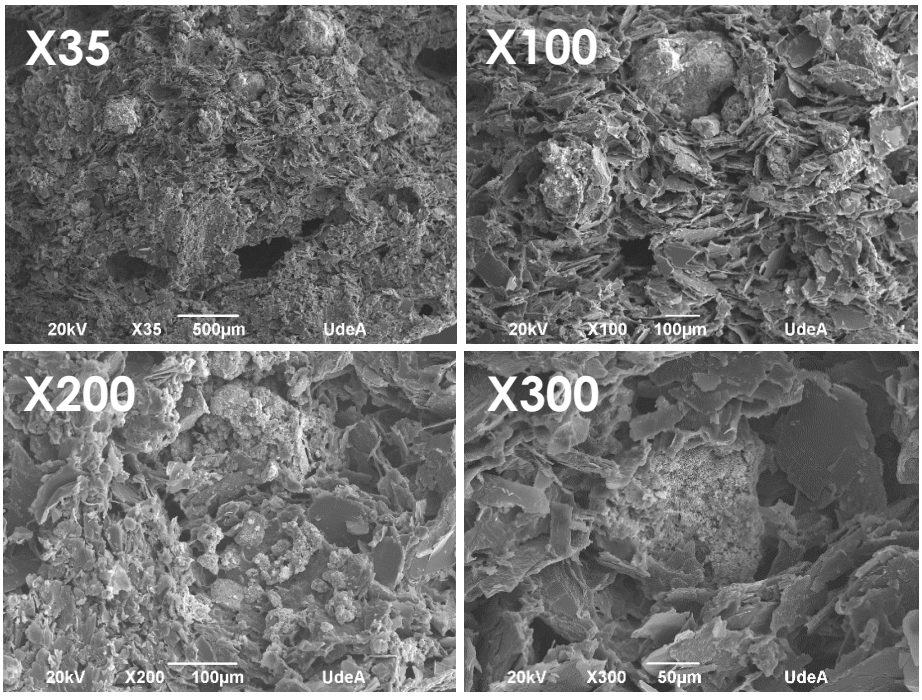

Figure 19. *SEM micrograph of specimen 10wt% BW*

Table 7 shows the percentage of the elements present in the specimen 10wt% BW. In the EDS mapping (see Figure 20) the distribution to a greater

extent of elements such as carbon, which is the constituent of the resin and the high content of graphite in the battery waste; chloride, manganese and zinc are elements present in a battery waste, and to a lesser extent elements such as aluminum, and silicon, elements relative to the other compounds of battery waste.

Table 7. *Composition of specimen 10wt% BW obtained by EDS*

	Element	C	Al	Si	Cl	Mn	Fe	Zn	Total
10wt%BW	(weight%)	75.18	1.20	1.57	3.93	4.78	1.66	11.68	100

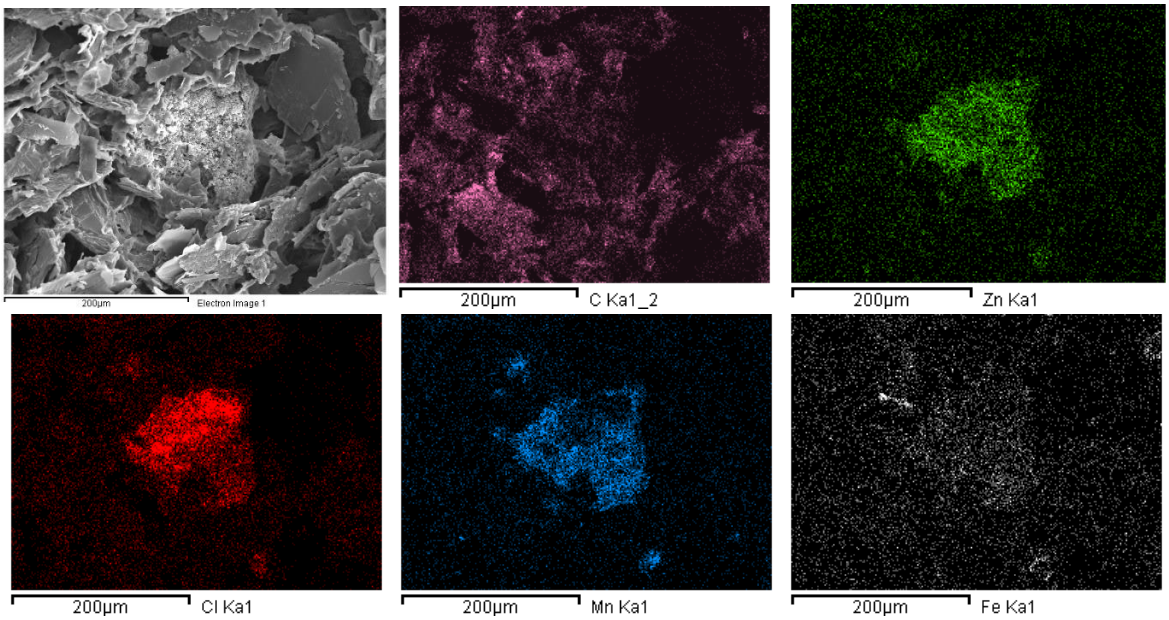

Figure 20. *EDS Mapping of specimen 10wt% BW*

Figure 21 represents the specimen with 15 wt% of BW, shows a better dispersion of the particles of the residue in the resin. This could be due to a better mixing process in the sample preparation and consequently, a more homogeneous distribution of BW was obtained.

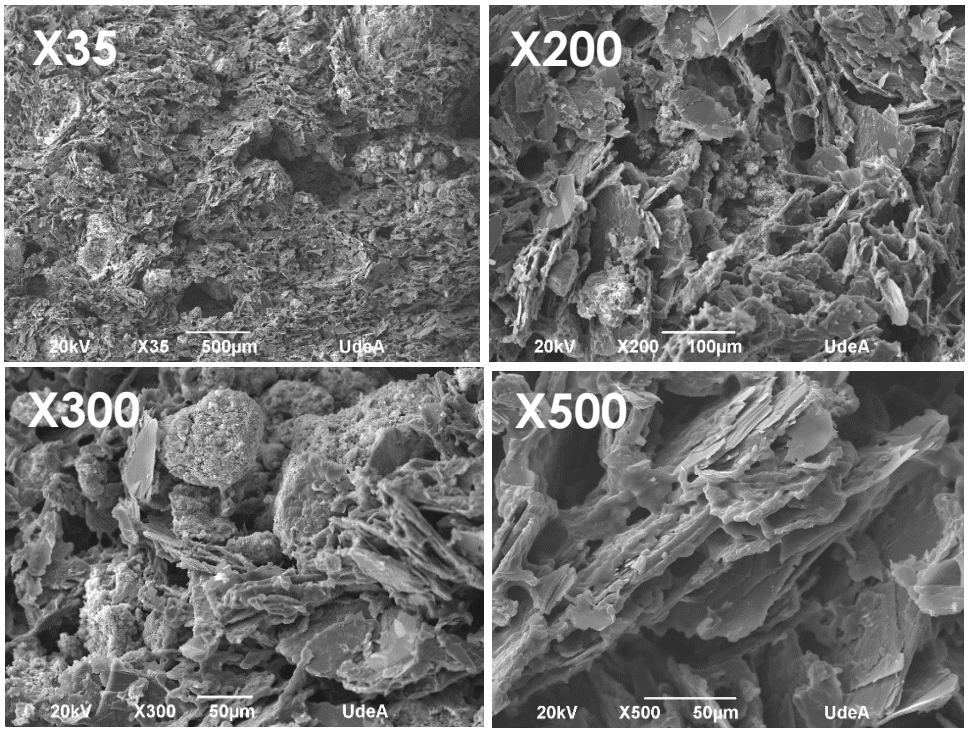

Figure 21. *SEM micrograph of specimen 15wt% BW*

Table 8 shows the percentage of the elements present in the specimen 15wt% BW. In the EDS mapping (see Figure 22) the distribution to a greater extent of elements such as carbon, which is the constituent of the resin and the high content of graphite in the battery waste; chloride, manganese and zinc are elements present in a battery waste, and to a lesser extent elements such as aluminum, and silicon, elements relative to the other compounds of battery waste.

Table 8. *Composition of specimen 15wt% BW obtained by EDS*

	Element	C	O	Al	Si	Cl	Mn	Fe	Zn	Total
15wt%BW	(weight%)	66.44	12.08	1.05	1.19	3.59	7.84	0.88	6.92	100

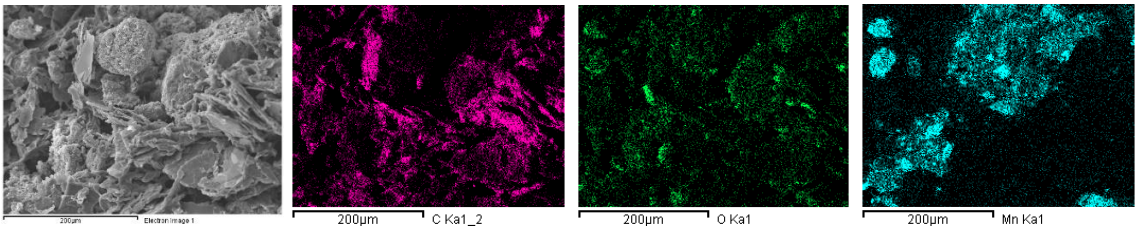

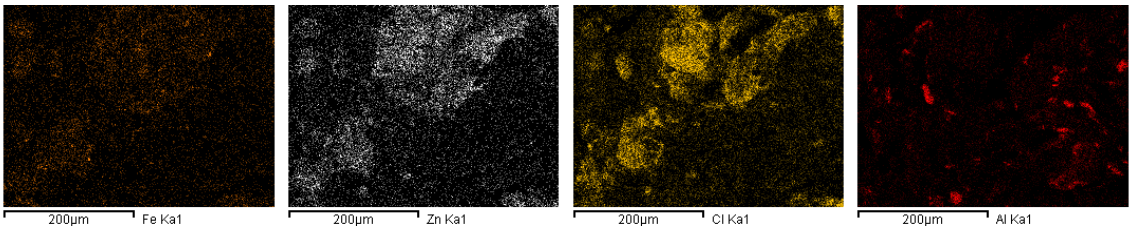

Figure 22. *EDS Mapping of specimen 15wt% BW*

Figure 23 represents the specimen with 20 wt% of BW. It shows a better dispersion of the battery residue in the resin. However, agglomeration of the residue and around the resin is observed, corresponding to the smooth part of the image. It can also be observed that the resin surrounds the agglomerations of the BW.

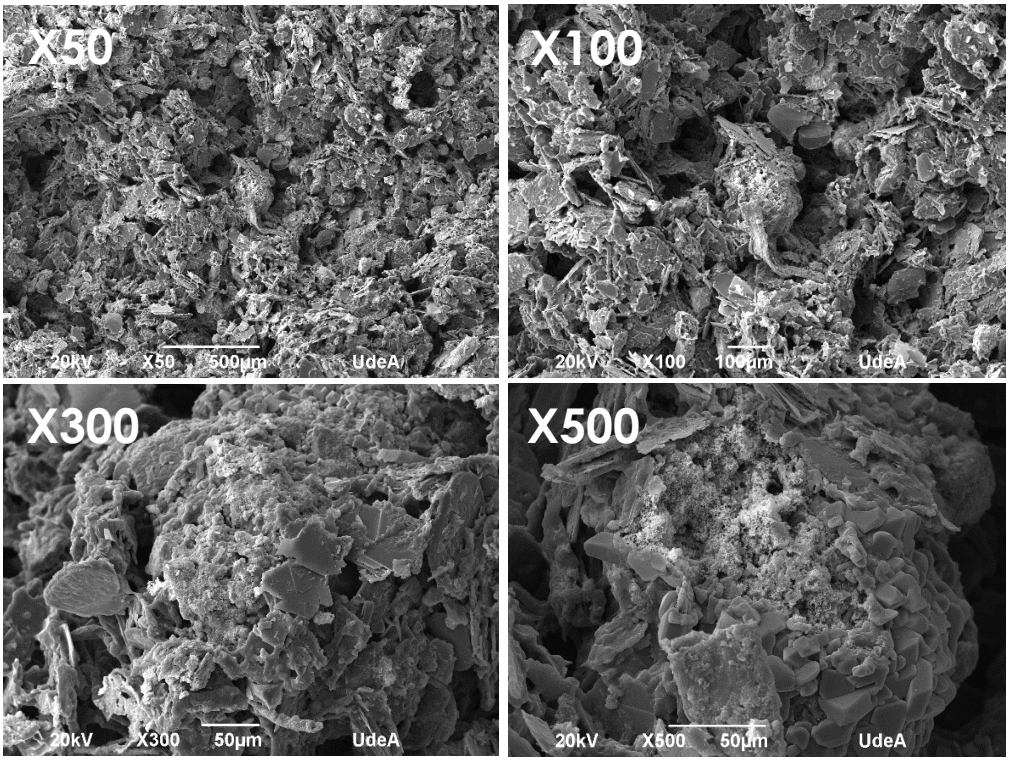

Figure 23. *SEM micrograph of specimen 20wt% BW*

Table 9 shows the percentage of the elements present in the specimen 15wt% BW. In the EDS mapping (see Figure 24) the distribution to a greater extent of elements such as carbon and oxygen, which is the constituent of the resin and the high content of graphite in the battery waste; In the part where the agglomeration of the battery waste particles is observed, manganese and zinc are concentrated, corresponding to the components

of the waste. Iron distribution is observed due to the conductive character of the resin. Chloride and aluminum are present too in a lesser extent.

Table 9. *Composition of specimen 20wt% BW obtained by EDS*

	Element	C	O	Al	Cl	Mn	Fe	Zn	Total
20wt%BW	(weight %)	44.67	12.04	1.43	3.62	21.42	1.13	15.68	100

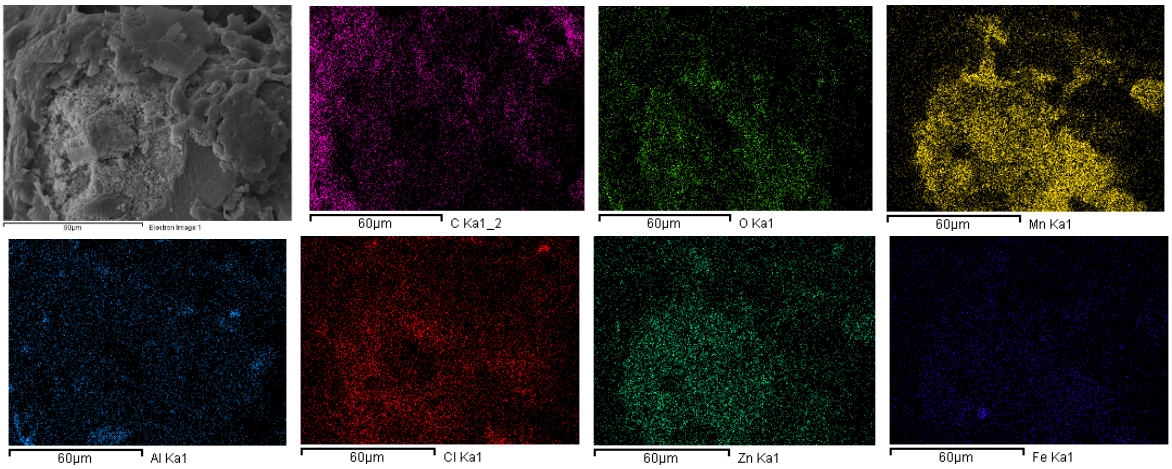

Figure 24. *Composition of specimen 20wt% BW obtained by EDS*

Figure 13 shows the particle size distribution of different specimens with resin and BW. For 5, 10, and 15% of residue, there is an increase in the average particle size, due to the agglomeration that occurs of the particles in the resin. The particle size of 5wt% BW specimen is on average 49.7 µm, this value is due to the agglomeration of particles of BW; the standard deviation is 11.2. The particle size of 10wt% BW is on average 16.5 µm and the standard deviation is 6.5. The particle size of specimens 15, and 20 wt% BW are 14.3 and 9.08 µm respectively showing a better dispersion of BW in the resin. Their standard deviations are around 5, which indicates that the particles in the composite material are about the same size.

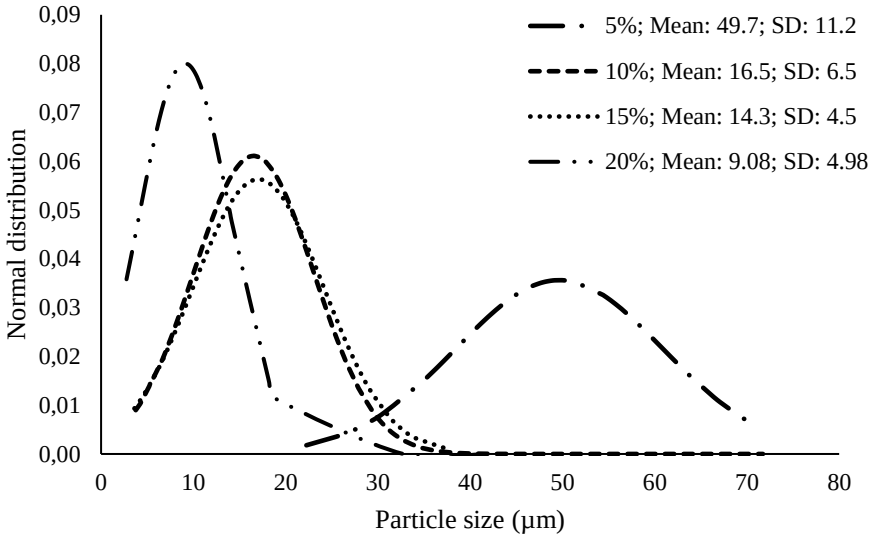

Figure 25. *Particle size distributions of specimens 5, 10, 15, and 20wt% BW*

5.2.2. FTIR Analysis

Figure 25 shows the FTIR spectrum for the specimen with 10wt% BW. The black color of the specimen makes detection in the infrared equipment challenging. The composite has no peak in the FTIR analysis. EDS in Figure 20 is the most suitable method of quantifying the chemical composition of the compound.

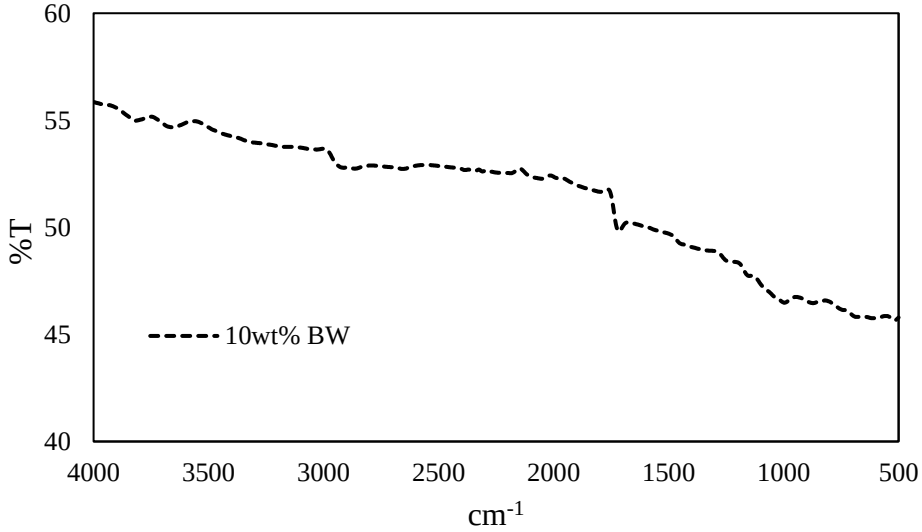

Figure 26. *FTIR for 10wt% BW composite*

5.3. Mechanical characterization

5.3.1. Hardness test

Shore hardness is a measure of the material's resistance to needle penetration by a given spring force. That is measured as a number from 0 to 100 on Scales A or D. The higher the number, the higher the hardness. Use letter A for flexible types and letter D for rigid styles [97]. The Shore D hardness scale is often used to measure soft or semi-soft elements. This test was used because the matrix composite material is polymeric. Polymeric materials such as rubbers, plastics, and elastomers are known to be soft elements. Figure 27 shows Shore D hardness test results, where clearly, as the BW contents increases, the hardness decreases as well. This may be associated with the waste particles occupying spaces. This can be associated to a higher graphite content and to an adverse effect of the ceramic powder reaction with the conductive polymer because it contributes to the material losing crystallinity and therefore, also losing hardness. In Figure 27, no significant differences between the hardness of the specimens with 10, 15, and 20% was evidenced. It must considered that the hardness of a polymeric material and other mechanical properties, there is a close relationship like with steel, that is, not necessarily a harder material, will have greater tensile strength [98].

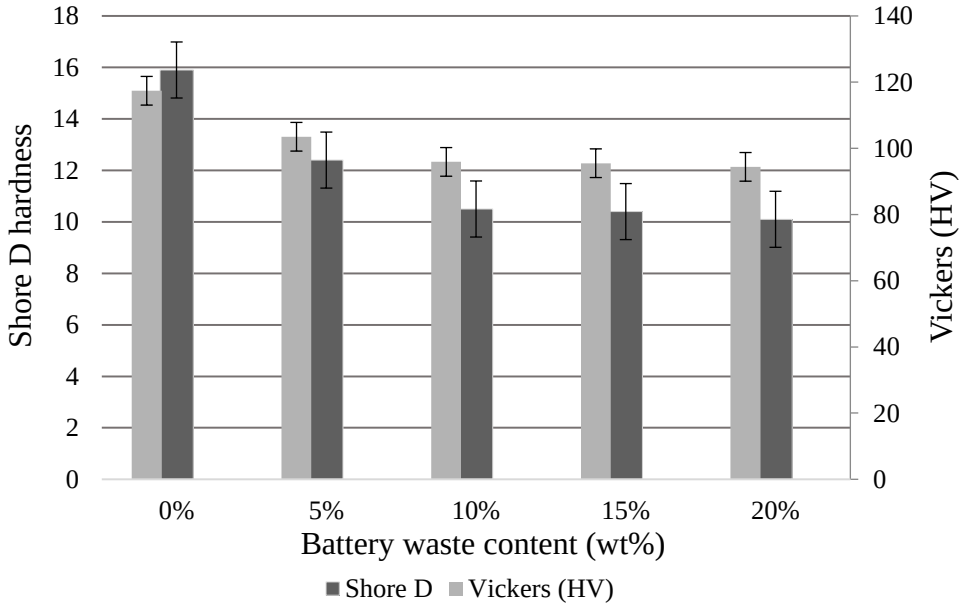

Figure 27. *Hardness results for the investigated specimens*

5.3.2. Density, compression tests and elastic modulus

Density tests were conducted over the specimens, where the resin has a density of 0.9 g/cm^3. With the addition of the residue, there is an increase in density in all formulations; this is because the mass of the battery waste powder occupies space in the resin generating an increase in the mass in the same volume. However, the increase of the density is only 0.1 g/cm^3. The density between the formulations has no significant differences and has a value of approximately 1 g/cm^3 (see Figure 28).

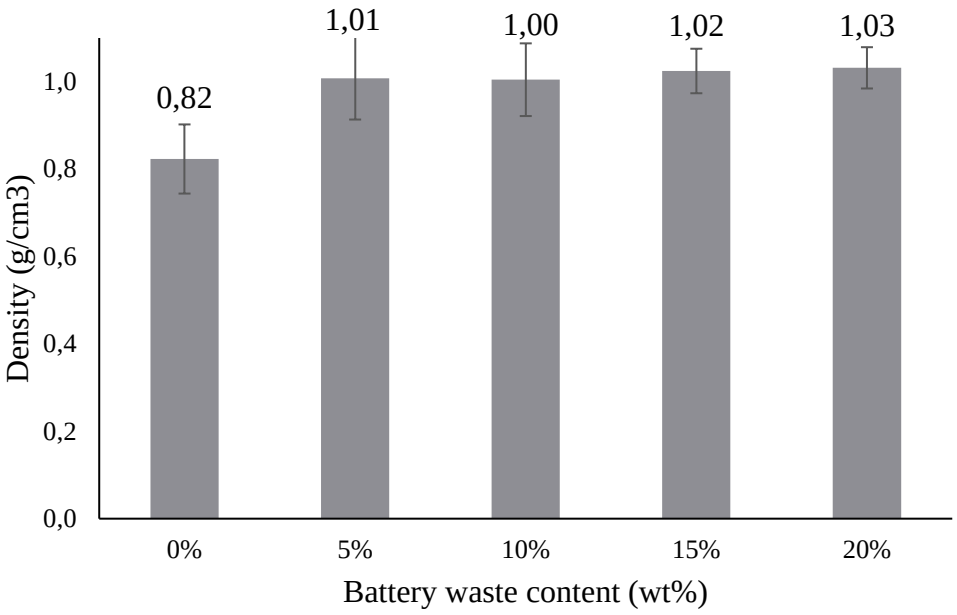

Figure 28. *Density of specimens*

Figure 29a shows typical stress-strain curves of the compressive tests for the specimens with 5wt% BW, 10wt% BW, 15wt% BW and, 20wt% BW. The 0wt% BW sample was not possible to test due to high shrinkage. As the percentage of residue increases, the compressive strength of the composite material increases as well. There were no significant differences between specimens 10wt% and 15wt% BW in the compressive strength. The specimen with 20wt% of BW has a higher compressive strength. As the specimens were compressed, the porosity decreases and leaves the particles closer together, which means that the greater the amount of residue, the greater the resistance to compression. In Figure 29a, the data is taken up to a 50% of deformation, where the curve presents an inflection point, because the amount of axial deformation affects the transverse deformations, generating

an increase in the contact area. At the beginning of the curve, between 0 and 0.2 of strain, the elastic zone of the material can be observed in the zoom. Figure 29b shows the elastic modulus obtained from the elastic zone. As the amount of battery residue increases, the modulus of elasticity increases too; meaning that the ceramic powder in the battery waste contributes to an increase in the material stiffness. Morphologically, this zone presents a linearity that does not imply dimensional changes to small deformations involved; however, this does not suggest that there are no transverse deformations at the beginning of the test, but they are so small that they do not influence the macroscopic behavior of the piece [99]. After the elastic zone, a change in the curve takes place that corresponds to the other zone where a classic expansion effect is observed in the elastic solids. After the linear range, deformations are generated in the longitudinal and transverse axes, generating a dimensional change in the contact area of the specimen, and generating irreversibility too [100]. The curve does not present a break, making it necessary to carry out dynamic mechanical behavior tests.

a)

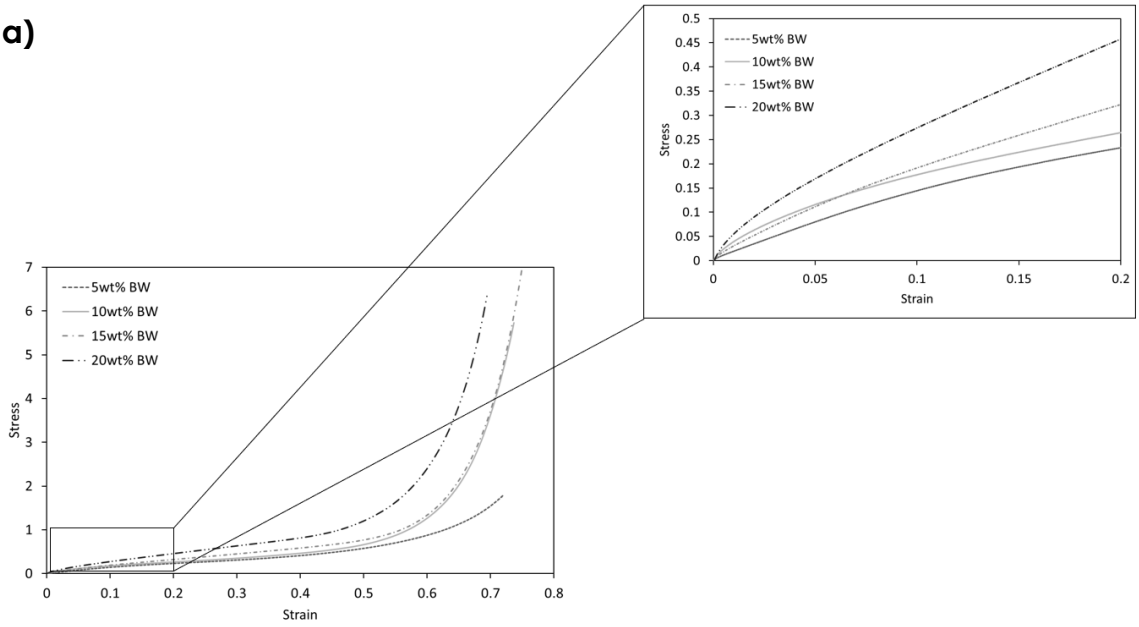

b)

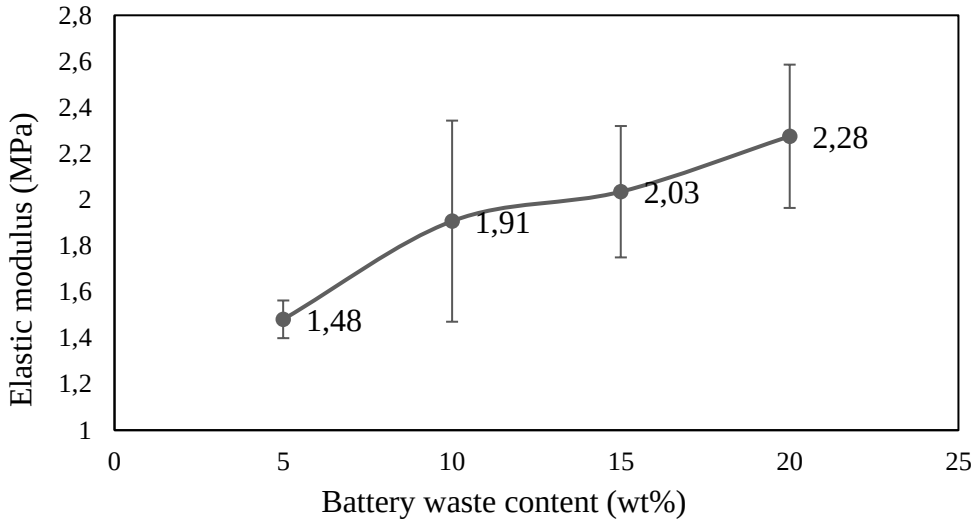

Figure 29. a) *Typical compression curves* ***b)*** *Elastic modulus*

Chapter 6

6. Conductivity of Composite Material

6.1. Results of piezoresistive tests

6.1.1. Electrical resistance

Sensor resistance was converted to a voltage signal via the implementation of a voltage divider circuit, putting the sensor in series with a fixed resistor R_L as shown in Figure 8b. The voltage measured in the junction of the sensor resistor is obtained by applying the law of Ohm, as shown in 2. From 2, the resistance is plotted against the force, thus, the equation for each piezoresistive sensor is obtained.

$$V_o = V_{in} * \left(\frac{R}{R_L} + R\right) \quad (2)$$

Where V_o is the output of the voltage divider, R_L is the resistance that completes the voltage divider, and V_{in} is the input voltage of the sensor.

Figure 30, Figure 31, and Figure 32 show two zones corresponding to a switch-like behavior and a power-law behavior until the saturation of the sensor. Switch-like or dynamic range refers to the significant variation in resistance between changes in force and it do not exhibit a constant change in resistance. Power-law refers to low changes in resistance when the force increases until, with an increasing force, the resistance does not show significant variations. These zones in each sensor depend on the residue concentration and the geometry of the electrodes (see Figure 8). In Figure 30, Figure 31, and Figure 32 the switch-like zone increases as the content of battery waste increase too. When residue concentration is higher, the stiffness is higher also (see Figure 29b), and the higher stiffness contributes to the saturation of the sensor with a greater force, but care must be taken

because it may have a higher risk of fracture. After this point, with small increases in force, saturation occurs more quickly causing a poor resolution in resistance on sensors with a smaller elastic modulus. Figure 30a shows that the sensor can reach a resistance of 82 ohm with 500 N applied, while in Figure 30b, Figure 30c, and Figure 30d it is observed that since saturation is slower, more force is required to reach to the same resistance. In the switch-like zone there is a larger difference between two points of resistance measured when the force is applied. As the battery residue content increases, the resistance increases under the same applied force and the difference between resistances is lower. Figure 31 shows that the switch-like behavior and power-law zone using geometry 2 has the same trend as geometry 1. However, the sensed resistance range is less, and the resistance value obtained at 500N is less than that obtained with the geometry 1. Figure 32 shows that the resistance range is less than with geometries 1 and 2 and has a faster saturation, this is because the sensor electrode geometry has a larger contact area. As the amount of battery residue increases, the resistance obtained at 500N is less. The power-law zone is where the sensor is stabilized and from that point on, the sensitivity of the sensor is obtained.

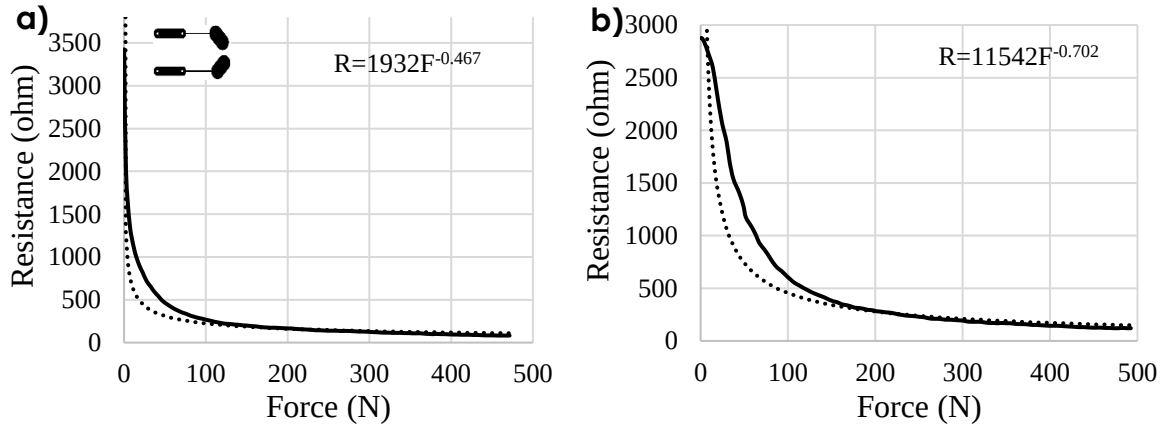

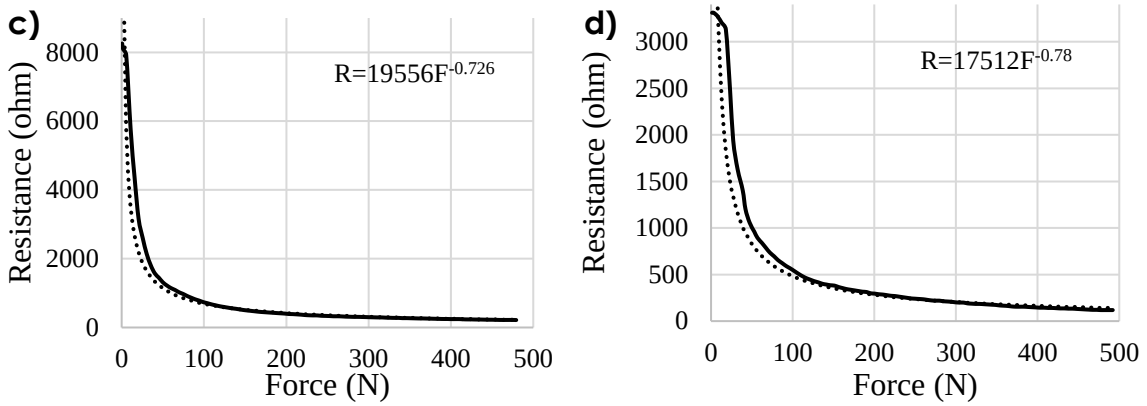

Figure 30. *Resistance vs. Force sensor geometry 1 (See Figure 8a) with different amount of battery waste* ***a)*** *5wt% BW* ***b)*** *10wt% BW* ***c)*** *15wt% BW* ***d)*** *20wt% BW*

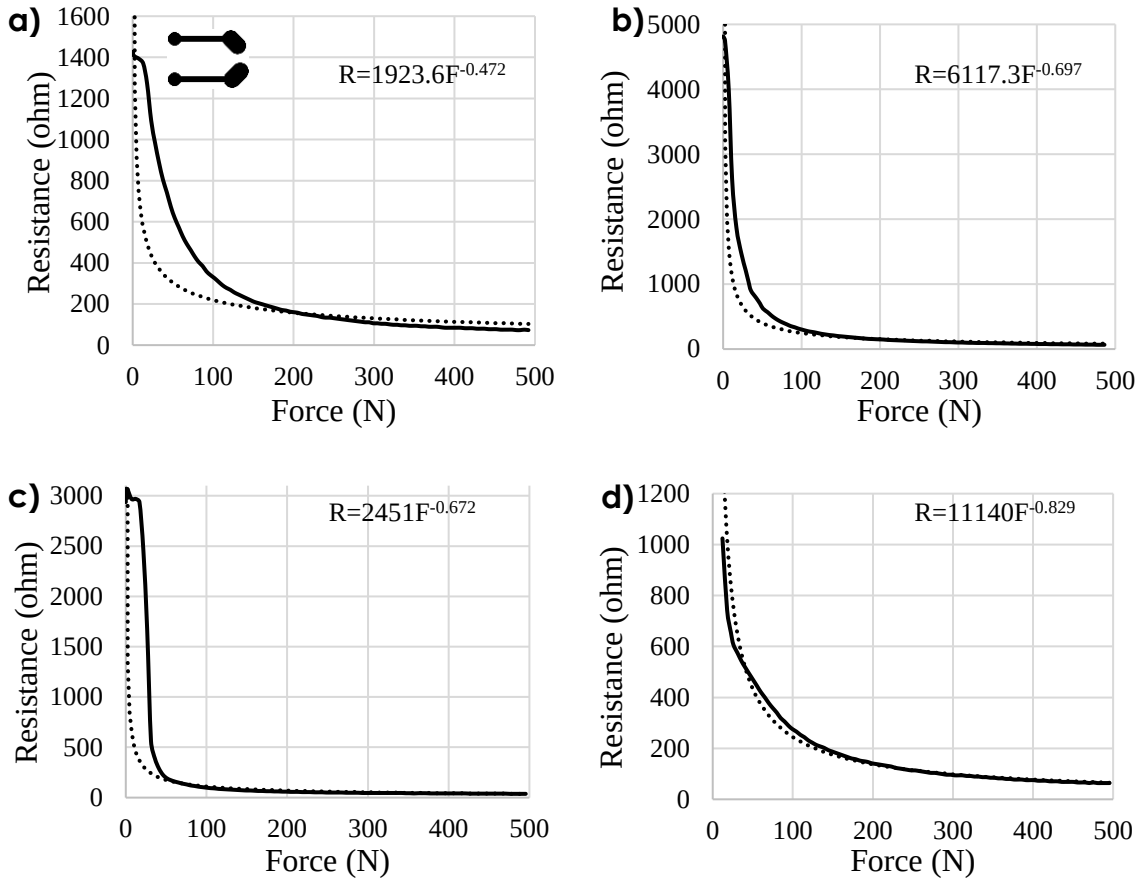

Figure 31. *Resistance vs. Force sensor geometry 2 (See Figure 8a) with different amount of battery waste* ***a)*** *5wt% BW* ***b)*** *10wt% BW* ***c)*** *15wt% BW* ***d)*** *20wt% BW*

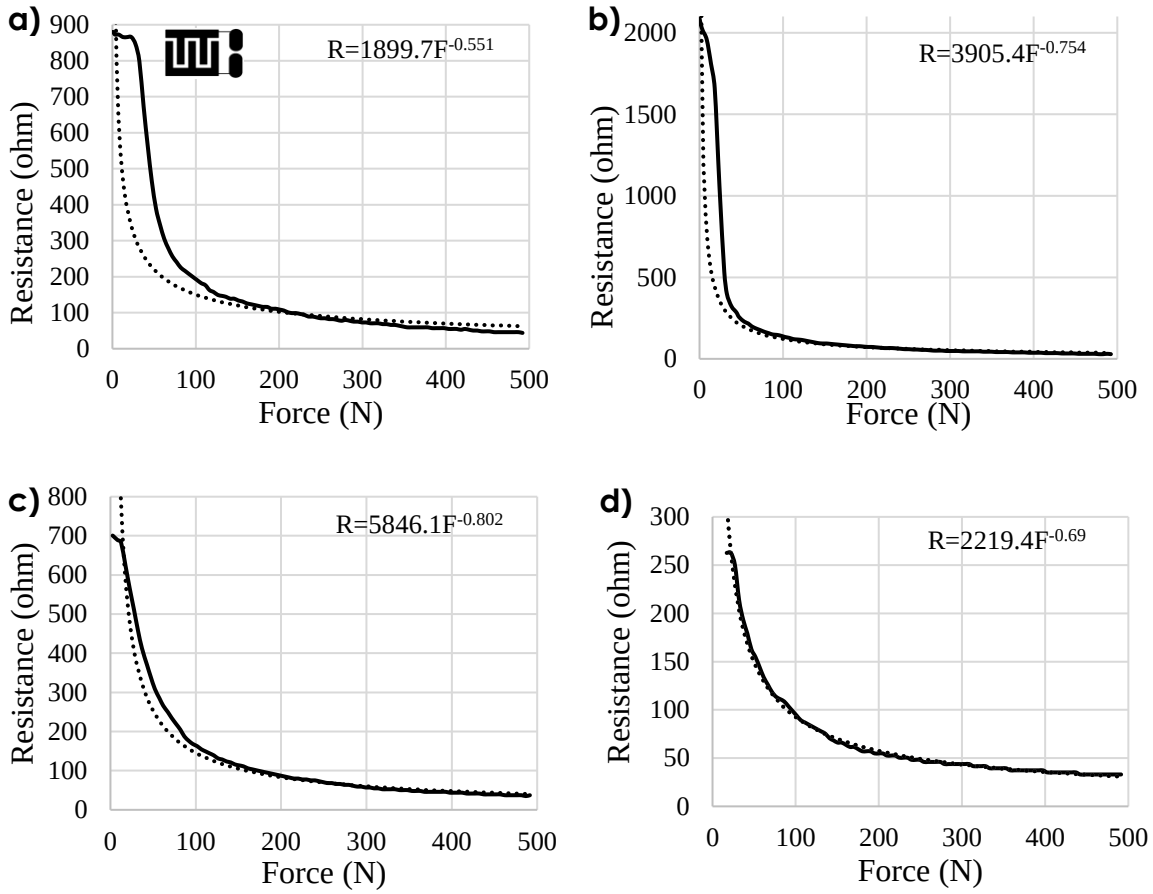

Figure 32. *Resistance vs. Force sensor geometry 3 (See Figure 8a) with different amount of battery waste* ***a)*** *5wt% BW* ***b)*** *10wt% BW* ***c)*** *15wt% BW* ***d)*** *20wt% BW*

6.1.2. Conductivity

The resistivity of the specimens (ρ) was calculated by 3.

$$\rho = \frac{R*A}{d} \quad (3)$$

Where ρ is the resistivity, R is the resistance of the specimen, d is the thickness and A the area of the electrodes. The electrical conductivity (σ) in S/m was calculated from the inverse of ρ [102]. The called percolation threshold is the critical value at which a sharp transition in conductivity occurs with a low rise in the content of the conductive charge [103]. In Figure 33 it is observed that the electrical conductivity increases when the amount of battery waste increase in the polymer matrix, but a stabilization is observed when the amount of battery waste is 10%. For the geometry 3, which has a greater

contact area, the conductivity increases as the battery residue increases, obtaining its maximum value with a concentration of 10%, then, the conductivity decreases. Percolation theory claims that there is a critical concentration (or percolation threshold) at which the mixture forms a conductive path that induces the transition from an insulator to a conductor [104], [105]. An inflection point of the conductivity curve can be observed around 5 wt% BW, and this is considered to estimate the percolation threshold. In the solid polymer composites, the conductive filler is distributed in a random orientation. The alignment in the polymer matrix is thus considered anisotropic [106].

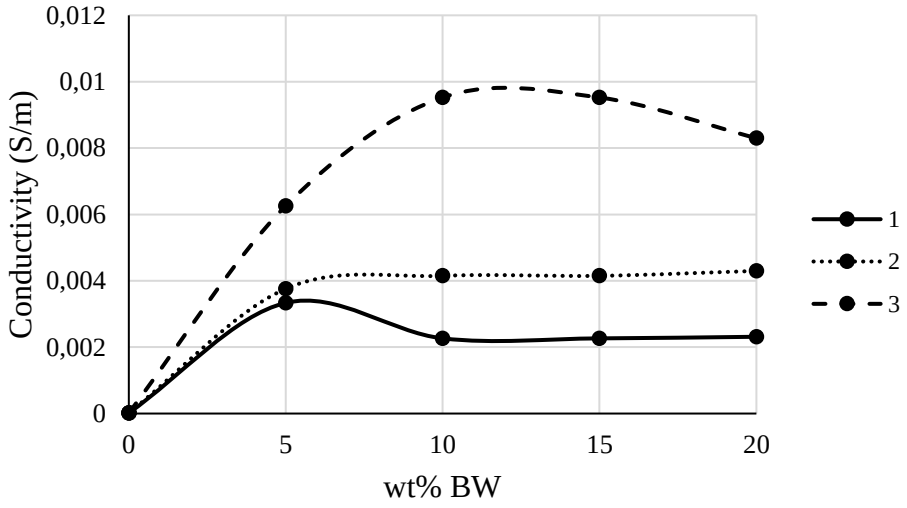

Figure 33. *Variation of electrical conductivity with different amount of battery waste*

Figure 34 shows the morphology of the filler in the polymer phase. Several studies have reported the effect of the aspect ratio of fillers on the electrical properties of polymer composites, in which the addition of high aspect ratio fillers significantly increases the electrical conductivity of polymer composites [102], [107]–[109]. The aspect ratio of the battery residue is low, a higher concentration is required to reach the percolation threshold.

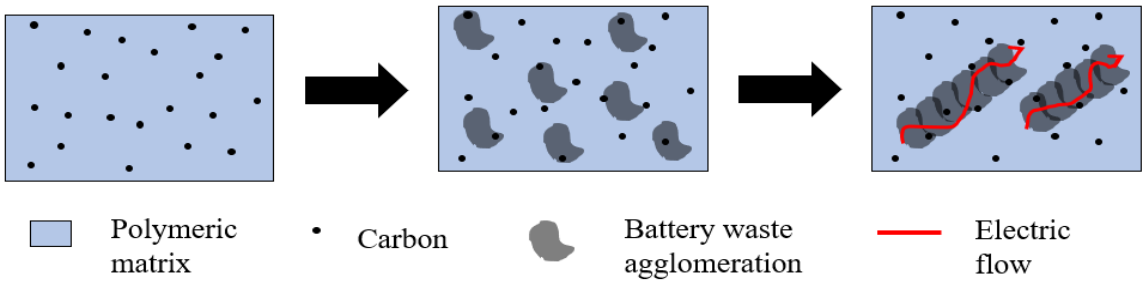

Figure 34. *Schematic mechanism of electrical conduction*

6.2. Characterization as a piezoresistive sensor

Piezoresistive composite materials can be obtained by compounding an insulating polymer with conductive fillers such as metal particle, carbon black, graphite power, and carbon fiber [107]–[110].

6.2.1. Sensitivity

Table 10 shows the sensitivity values of each sensor every 5N. All sensors have similar values of sensitivity; however, sensors with geometry 1 have the highest values of sensitivity and sensors with geometry 3 have the lowest values of sensitivity. For geometry 1, as the content of battery waste increase, sensitivity increase too. For geometry 2 and 3, as content of battery waste increase, the sensitivity decrease.

Table 10. *Sensitivity of sensors*

Geometry	wt% BW	Sensitivity (ohm/5N)
1	5	1.55
	10	1.95
	15	2.70
	20	2.29
2	5	1.24
	10	1.12
	15	0.48
	20	1.00
3	5	1.34
	10	0.96
	15	0.81
	20	0.48

6.2.2. Gauge factor

The gauge factor *GF* is defined in terms of its mechanical and electromechanical properties. The gauge factor is calculated using equation 4. The value of the gauge factor is influenced by the variation of the piezoresistive conductor resistivity and by the variations in its dimensions (longitudinal and transverse) caused by its lengthening, depending on the Poisson ratio [111].

$$GF = \frac{\frac{\Delta R}{R_0}}{\varepsilon} \quad (4)$$

Where *GF* is the gauge factor, ΔR is the change of resistance, R_0 is the initial resistance, and ε is the strain. For elastomers, the Poisson's ratio is generally close to 0.5; GF values >2, therefore, reflects contributions from piezoresistivity [112]. According to the gauge factor of all the samples presented in Table 11, the material presents piezoresistive properties.

The gauge factor is used to compare the difference in sensitivity of different piezoresistive sensors. In this way it is determined that piezoresistive sensors are very relevant due to their low cost, easy manufacturing and measurement, and high sensitivity [113]; they are also more flexible than semiconductors [114] and their sensitivity is higher than that of sheet metal trade. Literature reports nanocarbonaceous/poly(vinylidene fluoride) composites with sensibilities that depend on the nanocarbonaceous aspect ratio, where GF varies between $0.5 < GF < 10$. A larger aspect ratio of nanocarbonaceous shows larger sensibility in polymer composites [115]. Different composite materials have been developed with piezoresistive applications showing a gauge factor range from 0.99 to 2.36 using a styrene polymer matrix and carbon nanotubes as reinforcement [116], [117].

It may be noted that GF is only one of the several criteria for strain sensing applications, and strain sensors with GF as low as 0.82 can be used human motion detection [118]. The integration of tensoresistors with objects in different applications warrants different physicomechanical and electromechanical characteristics. For example, tactile sensing demands low Young's modulus sensors whereas structural health monitoring sensors will benefit from higher values of Young's modulus [119], [120]. It is therefore important to have tensoresistive materials with different physicomechanical attributes [118].

Table 11. *Gauge Factor of sensors*

Geometry	wt% BW	GF
1	5	4.70
	10	3.88
	15	5.76
	20	4.43
2	5	2.03
	10	4.24
	15	6.25
	20	3.65
3	5	2.57
	10	4.49
	15	4.79
	20	8.88

6.3. Statistical analysis

The statistical analysis was performed in RStudio software. Figure 35 shows that the results obtained from resistivity, final resistance, and sensor sensitivity are not uniformly distributed. Figure 35a shows that the resistivity of the sensors is more dispersed after reaching 1537 kΩ, for higher values, the resistivity values are closer. Figure 35b shows that the final resistance values are more evenly distributed compared to resistivity and sensitivity, and have a smaller range, meaning that the sensors have similar final resistance values respect to the applied force, but it exhibits a very high atypical data. Figure 35c shows that the sensitivity values are not uniformly distributed. The sensitivity of the sensors varies between 0.5 and 2.7 and most sensors have a sensitivity greater than 1. Figure 35d shows that the gauge factor is almost uniformly distributed between 2 and 6.5, except by one atypical point in 8.

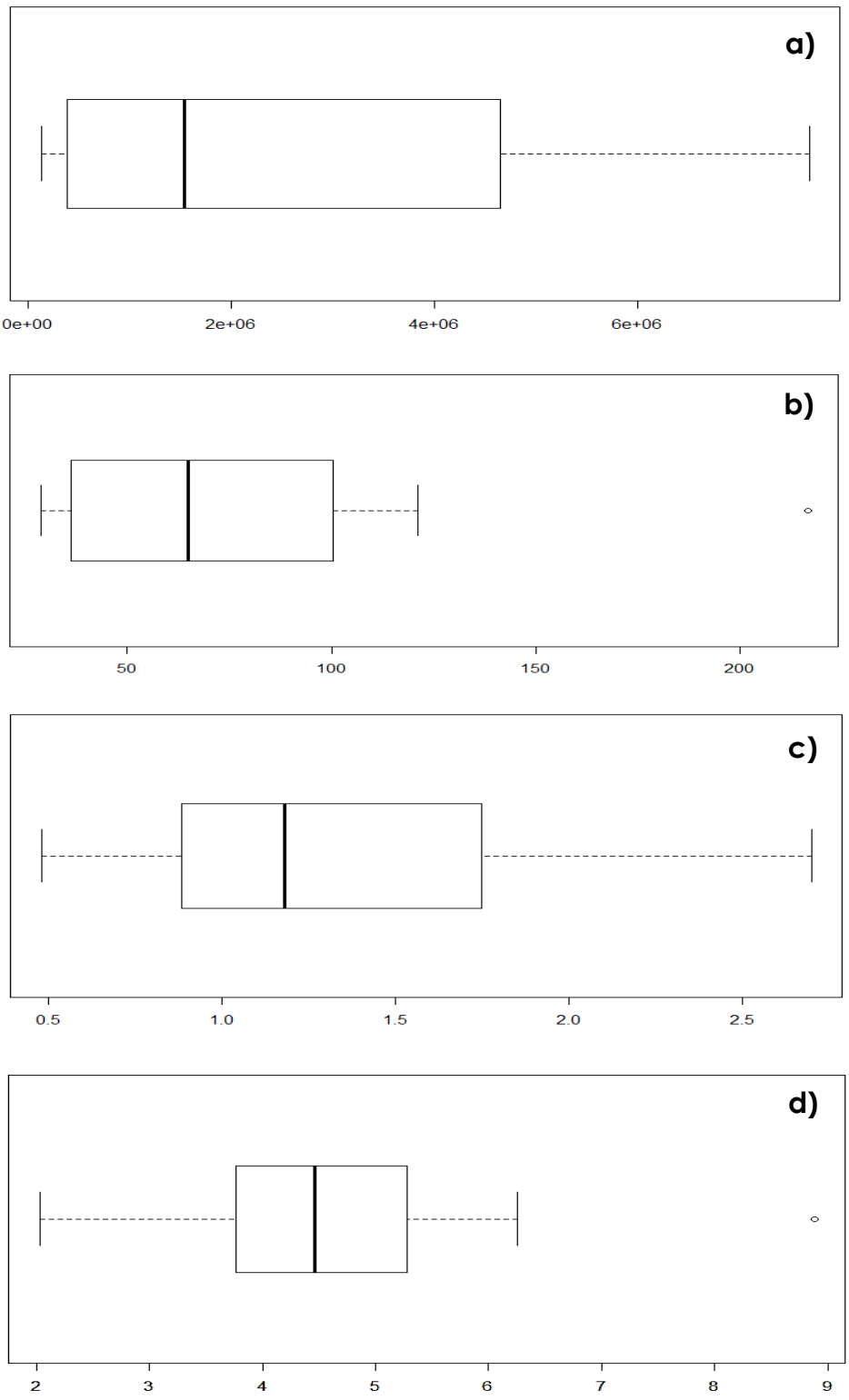

Figure 35. *Boxplot of* ***a)*** *Resistivity* ***b)*** *Final resistance* ***c)*** *Sensitivity* ***d)*** *Gauge factor*

Equations of regression have been obtained for the effect of individual variables and their relative importance in the process. The effects of the variables were fitted using a generalized linear model in the RStudio software with the data of resistivity, final resistance, sensitivity, and gauge factor obtained. The consistency of the model's fit was assessed using ANOVA and meaning test. Mathematical model form is

$$Y = X_0 + X_1 * \alpha + X_2 * \beta \quad (5)$$

Where Y is the predicted value of response, X_0 is the independent term, X_i is the regression coefficients, which show the effect of the corresponding parameters, a represents the amount of battery waste (wt%), and β corresponds to type of geometry (G). An empirical relation between the independent variables according to the experimental results (wt% battery waste and geometry) and the responses resistivity, final resistance, and sensitivity) are given in terms of actual values. Table 12 shows the equations of the mathematical models for resistivity, final resistance, and sensitivity using the different geometries 1, 2, and 3.

Table 12. *Mathematical models for resistivity, sensitivity, final resistance, and gauge factor*

Geometry	**Equations**
Geometry 1	*Resistivity = 390.995 + 310.997 wt%BW*
	Sensitivity = 2.216 - 0.007 wt%BW
	Final Resistance = 124.42 + 0.81 wt%BW
	GF = 2.43 + 0.18 wt%BW
Geometry 2	*Resistivity = 390.995 + 310.997 wt%BW - 2052542 G2*
	Sensitivity = 2.216 - 0.007 wt%BW - 1.162 G2
	Final Resistance = 124.42 + 0.81 wt%BW - 74.55 G2
	GF = 2.43 + 0.18wt%BW - 0.65 G2
Geometry 3	*Resistivity = 390.995 + 310.997 wt%BW - 2987269 G3*
	Sensitivity = 2.216 - 0.007 wt%BW - 1.225 G3
	Final Resistance = 124.42 + 0.81 wt%BW - 99.38 G3
	GF = 2.43 + 0.18wt%BW + 0.49 G3

Assessment of degree of significance is estimated for resistivity, final resistance, and sensitivity. To analyze the models, an analysis of variance (ANOVA) was performed to determine the importance of the effects and interactions between variables. The summarized ANOVA results are given in Table 13, Table ***15***, Table 17, Table 19, respectively, for resistivity, final resistance, gauge factor and sensitivity. To verify the fit of the models

obtained, the Hosmer-Lemeshow test was used, which evaluates the distance between what is observed in the data obtained and what is expected under the model. The null hypothesis indicates that there are no differences between the observed values and the predicted values, so if the P-value > 0.05, the null hypothesis is accepted. Table 21 shows the P-values of the adjusted models for resistivity, final resistance, sensitivity, and gauge factor, and all P-values are greater than 0.05, therefore, indicating an appropriate fit of the models to the experimental data. According to Table 14, for the resistivity, the factor that has the greatest importance is the amount of battery residue and has a directly proportional value. Regarding to the final resistance, Table 16 shows that the factor that most affects this property is geometry, especially geometry 3. Figure 8a shows that geometry 3 is the electrode that has the largest contact area, which can be related to the influence on the final resistance of the sensor. Table 18 shows that the sensitivity is affected by the geometry. Table 20 shows that the geometry does not affect the gauge factor. The amount of battery waste does affect; however, its value is not very significant.

Table 13. *ANOVA Table for resistivity*

	Df	Deviance Resid.	Df	Resid. Dev	F	Pr(>F)
wt%BW	1	3.6270e+13	10	4.739e+13	10.1066	0.01302
Geometry	2	1.8681e+13	8	2.871e+13	2.6027	0.13470

Table 14. *Regression coefficients and P-values for each factor (Resistivity)*

Term	Coefficient	P -Value
Intercept	390,995	0.8068
wt%BW	310,997	0.0130
Geometry 2	-2,052,542	0.1640
Geometry 3	-2,987,269	0.0563

Table 15. *ANOVA Table for final resistance*

	Df	Deviance Resid.	Df	Resid. Dev	F	Pr(>F)
wt%BW	1	249.3	10	31,902	0.190	0.67445
Geometry	2	21,402.5	8	10,499	8.154	0.01173

Table 16. *Regression coefficients and P-values for each factor (Final Resistance)*

Term	Coefficient	P -Value
Intercept	124.4175	0.00297
wt%BW	0.8154	0.67445
Geometry 2	-74.5517	0.01958
Geometry 3	-99.3845	0.00468

Table 17. *ANOVA Table for sensitivity*

	Df	Deviance Resid.	Df	Resid. Dev	F	Pr(>F)
wt%BW	1	0.0209	10	5.2238	0.1181	0.739930
Geometry	2	3.8079	8	1.4158	10.7580	0.005397

Table 18. *Regression coefficients and P-values for each factor (Sensitivity)*

Term	Coefficient	P -Value
Intercept	2.2158	0.000198
wt%BW	-0.00747	0.739930
Geometry 2	-1.1625	0.004494
Geometry 3	-1.225	0.003353

Table 19. *ANOVA Table for gauge factor*

	Df	Deviance Resid.	Df	Resid. Dev	F	Pr(>F)
wt%BW	1	12.3035	10	22.428	4.9682	0.05639
Geometry	2	2.6163	8	19.812	0.5282	0.60887

Table 20. *Regression coefficients and P-values for each factor (Gauge factor)*

Term	Coefficient	P -Value
Intercept	2.43	0.0954
wt%BW	0.18	0.0564
Geometry 2	-0.65	0.5752

Term	Coefficient	P -Value
Geometry 3	0.49	0.6713

Table 21. *Hosmer-Lemeshow goodness of fit test*

Term	P-value
Resistivity	1
Final Resistance	1
Sensitivity	0.6825
Gauge Factor	1

Chapter 7

7. Copper as Additive in the Composite Material

7.1. Materials and manufacture of composite material with copper

Battery waste powder was previously obtained from a local provider at Medellín. This waste resulted after grinding alkaline and Zn-C batteries with 0.2 µm. The waste is a black powdered mix, mainly composed of ZnO, MnO_2 and graphite particles [6].

The conductive polymer is a styrene vinyl acrylic resin with carbon particles obtained from Voltec Electrónica, Colombia.

UTP wire 0.5106 mm (24 AWG) in diameter and 100% copper and copper jumper wire 0.3211 mm (28 AWG). The copper wire was cut into 2mm pieces to ensure that it does not exceed the critical length i.e. 4 mm height of the samples.

Four different wire weights fraction contents were explored in the 5%wtBW composite material: 0, 5, 10, and 15%wt copper wire (CuW). The mixing of materials was conducted manually for few minutes. An aluminum mold of 12 mm in diameter and 4 mm in height was used to prepare samples for characterization and electrical tests. The samples were left at room temperature for about 48 hours, until they hardened completely. The experimental design is shown in Table 22.

Table 22. *Design of experiments composite material with additive*

Sample	Composite (%wt)	Copper wire (%wt)
Cu0	100	0

Sample	Composite (%wt)	Copper wire (%wt)
Cu1	95	5
Cu2	90	10
Cu3	85	15

7.2. Characterization

7.2.1. Density

When the specimens dried completely, their dimension of radius and height was obtained using a Vernier caliper. Density was determined by the dimensional method, in which measurements of height and diameter of the specimens were taken. A high precision Mettler Toledo balance was used to weight the specimens.

Density results are presented in Figure 36. The density of the specimen that is only the composite 5wt%BW is 0.94 g/cm^3. With the addition of the copper wire, there is an increase in density in all formulations. The above trend can be attributed to the fact that higher density in the composites is due to the presence of copper wires. The density of specimens is: 1.05, 1.10, and 1.20 g/cm^3, Cu1, Cu2, and Cu3, respectively.

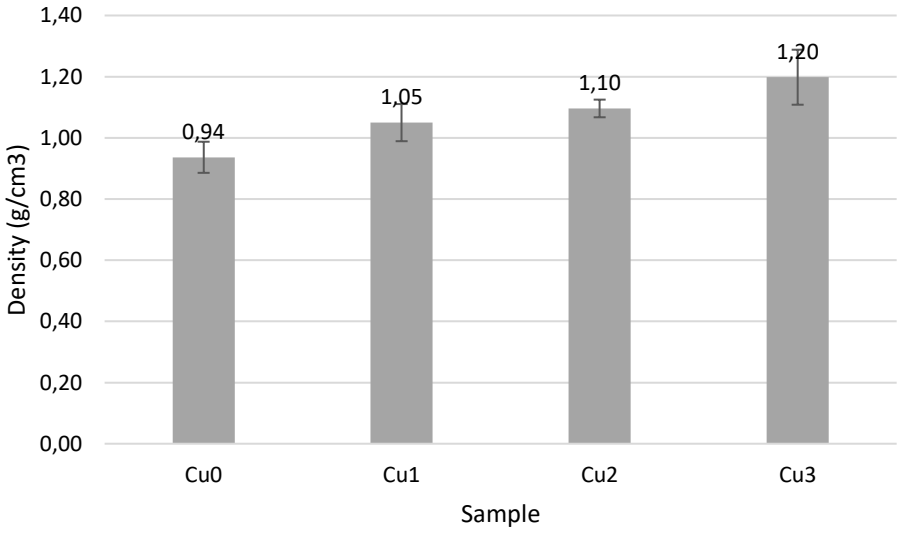

Figure 36. *Density of composite material with copper wire*

7.2.2. SEM

Scanning electron microscopy (SEM) and energy dispersive spectroscopy (EDS) were used to analyze the specimens in a JEOL JSM 6700R microscope operated in high vacuum mode. To specimen Cu0 (composite material 5wt%BW), it was cryogenized and then mounted on carbon tape and gold sputtered with a Hummer 6.2 apparatus at 15 mA AC for 30 sec to obtain a thin gold film.

In some areas, the battery waste is more concentrated, even agglomerated, which can be seen in Figure 37 which is the specimen with 5 wt% of BW. The agglomeration can be explained by the difficulty in the mixing process, which generates a poor dispersion of the residue in the mix. Carbon particles appeared, mostly, as imbibed particles in the matrix. A lot of graphite can be seen.

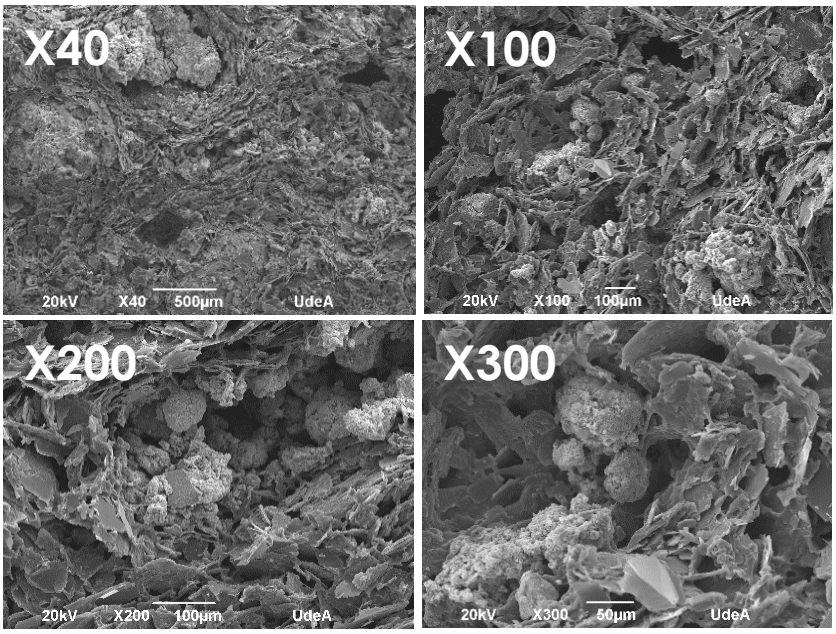

***Figure 37**. SEM micrograph of specimen 5wt% BW*

Figure 38 represents the specimen with composite material and 5wt%CuW, the micrograph shows cracks due to the high shrinkage of the resin and the residue surrounds the wire in the specimen. When the image is taken with a magnification of 2000X, it is observed that the smooth part is the polymeric matrix of the composite material. With the magnification of 5000X you can see the battery residue attached to the copper wire. Using the ImageJ software, the percentage of cracks with respect to the total area is 35%. The

corresponding graphite flakes can also be seen in the figure, especially in the upper left corner and the lower right corner with a magnification of 100X.

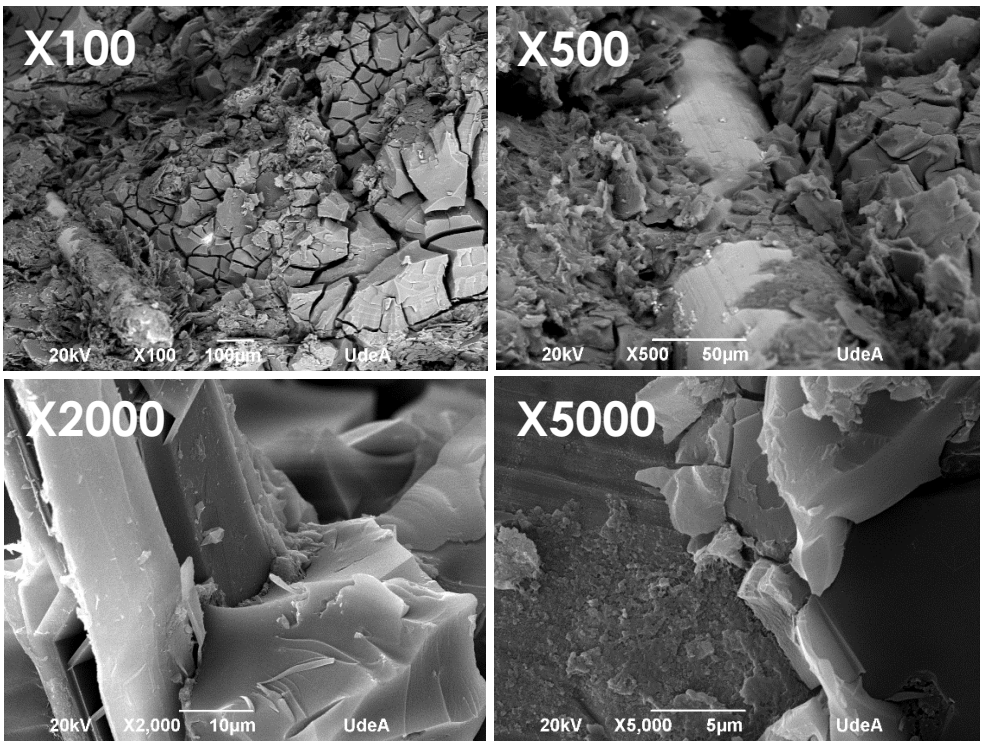

Figure 38. *SEM micrograph of specimen Cu1*

Table 23shows the percentage of the elements present in the specimen Cu1. In the EDS mapping (see Figure 39) the distribution to a greater extent of elements such as carbon and oxygen, which are the constituent of the resin and the high content of graphite in the battery waste; chloride, manganese, magnesium, and zinc are elements present in a battery waste, and to a lesser extent elements such as aluminum, and silicon, elements relative to the other compounds of battery waste. The composition shows a little percentage of copper that corresponds to the wire used as additive in the material.

Table 23. *Composition of specimen Cu1 obtained by EDS*

	Element	**C**	**O**	**Al**	**Si**	**Cl**	**Mn**	**Fe**	**Zn**	**Cu**	**Mg**
5wt%Cu	(weight%)	37.18	24.74	12.51	0.57	0.55	2.52	2.77	2.02	2.16	0.21

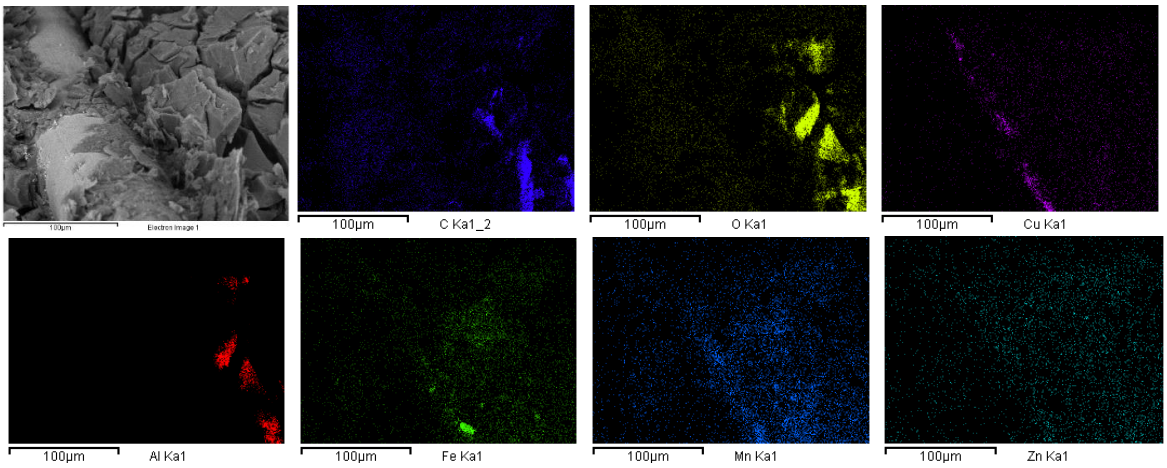

Figure 39. *EDS Mapping of specimen Cu1*

Figure 40 represents the specimen with composite material and 10wt%CuW, shows that there is no definite orientation for copper cables. It is also observed that the size of the cracks grows, with respect to the sample that has 5wt% CuW, thus, the percentage of free space that these samples present is approximately 40%.

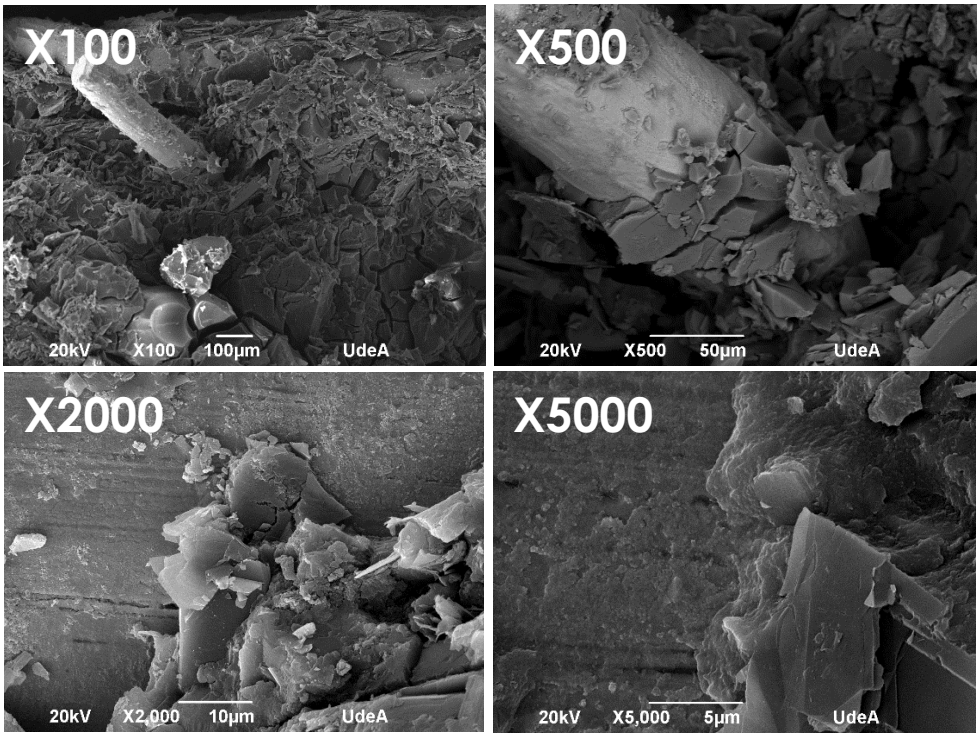

Figure 40. *SEM micrograph of specimen Cu2*

Table 24 shows the percentage of the elements present in the specimen Cu2. In the EDS mapping (see Figure 41) shows a significant increase in the amount of copper content, due to the fact that the percentage of cable added increased. The distribution shows a greater extent carbon and oxygen too, which are the constituent of the resin and the high content of graphite in the battery waste; chloride, manganese, magnesium, iron, and silicon, are present too.

Table 24. *Composition of specimen Cu2 obtained by EDS*

	Element	C	O	Al	Si	Cl	Mn	Fe	Cu	Mg	Total
10wt%Cu	(weight%)	28.71	11.94	10.89	0.36	0.15	0.92	0.72	46	0.32	100

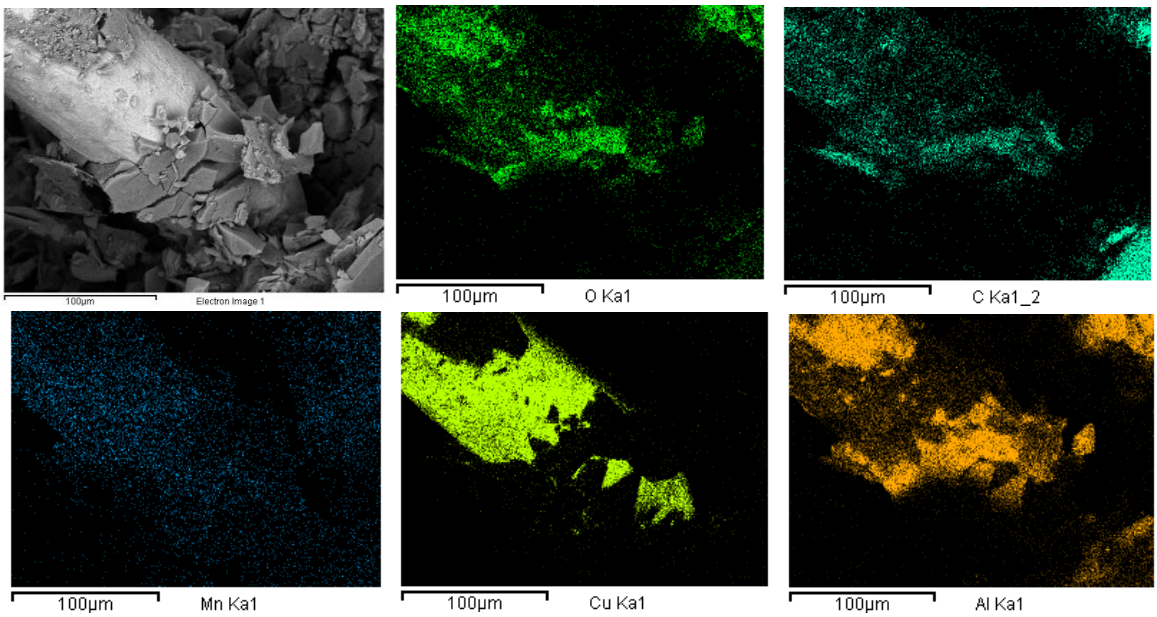

Figure 41. *EDS Mapping of specimen Cu2*

Figure 42 represents the specimen with composite material and 15wt%CuW, It is shown that the wires are distributed throughout the material and that those with a smaller diameter are better compacted within the material, while those with a larger diameter are seen passing through the material. In this composition there is a better dispersion of the resin and cracks decrease, however, the material is organized as flakes.

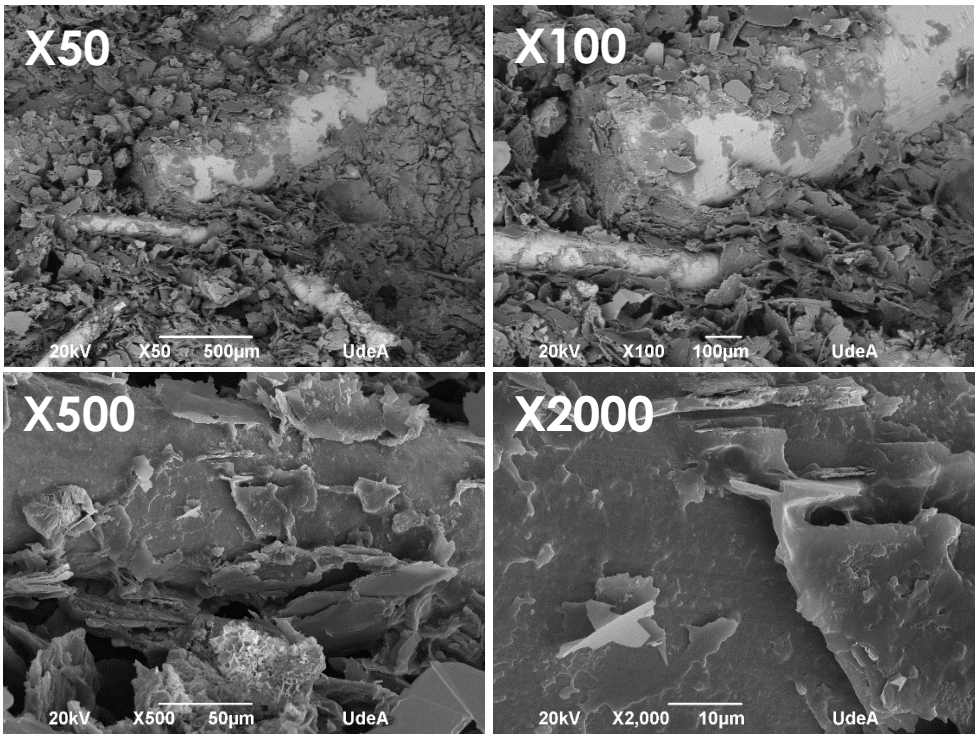

Figure 42. *SEM micrograph of specimen Cu3*

Table 24 shows the percentage of the elements present in the specimen Cu3. In the EDS mapping of the Cu3 specimen (see Figure 43), it can be observed that the highest content is the copper corresponding to the increase in the concentration of pieces of cable as an additive. The other elements that appear in the mapping correspond to metals of the battery waste such as zinc, aluminum and manganese and the components of the resin iron and oxygen.

Table 25. *Composition of specimen Cu3 obtained by EDS*

	Element	O	Al	Si	Ni	Mn	Fe	Cu	Zn	Total
15wt%Cu	(weight%)	6.83	3.63	3.36	0.96	1.84	30.35	47.73	5.29	100

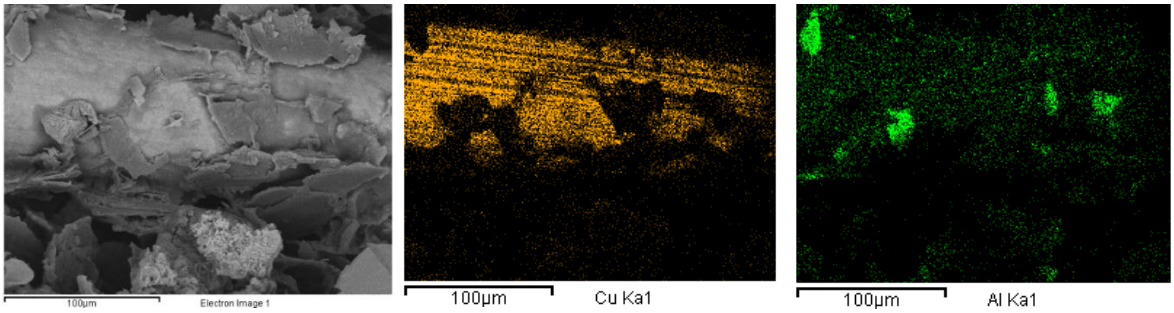

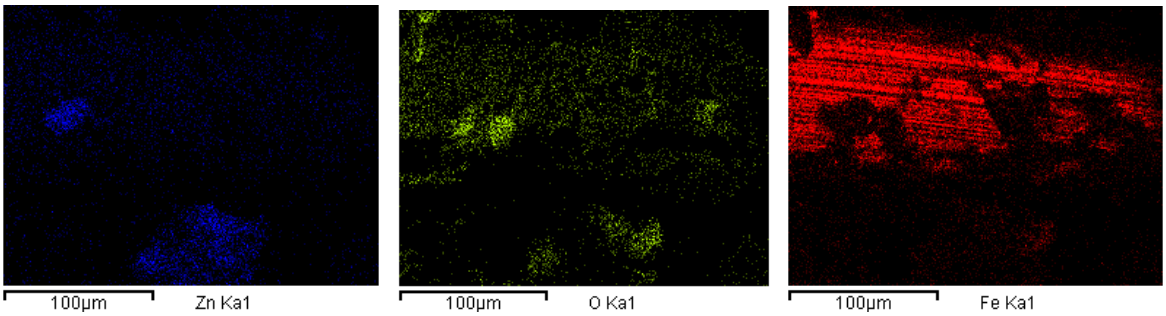

Figure 43. *EDS Mapping of specimen Cu3*

7.3. Electrical tests

7.3.1. Methodology

Piezoresistive tests were carried out with the sensors with copper as additive using geometry 1 (see Figure 8a), since according to the Table 10, it is the geometry that has the best sensitivity compared to 2 and 3. In addition, the percolation threshold is also given with 5wt% BW. This geometry has a contact area intermediate between 2 and 3. Circuits were constructed using the electrodes with specimens 5, 10, and15wt%CuW. Finally, compression tests were performed using a Shimadzu AG250KN universal testing machine (see Figure 8c). Both the configuration of the universal machine and the data acquisition system followed the same methodology as in section 6.1.1. of this document.

7.3.2. Results

Sensor resistance was converted to a voltage signal via the implementation of a voltage divider circuit, putting the sensor in series with a fixed resistor R_L as shown in Figure 8b. The voltage measured in the junction of the sensor resistor is obtained by applying the law of Ohm, as shown in 2. From 2, the resistance is plotted against the force, thus, the equation for each piezoresistive sensor is obtained.

$$\boldsymbol{V_o = V_{in} * \left(\frac{R}{R_L} + R\right)} \quad (6)$$

Where V_o is the output of the voltage divider, R_L is the resistance that completes the voltage divider, and V_{in} is the input voltage of the sensor.

Figure 44a, b, c, and d show the behavior of the resistance with respect to the applied force in the sensors that contain the composite material and

different amounts of copper wire as additive. It can be seen that the behavior of these sensors is completely different from those that are only made with the composite material. Sensors with the additive show linear trends, while those with only composite material show potential behaviors. Table 26 shows the differences in the R^2 of the different regressions in the settings of each sensor. This linear behavior is very important in sensor calibration, as they contribute to a more accurate sensor output, this implies that the use of an additive allows the sensor to be used without the need for corrections by means of other algorithms or calibrations [121]–[123]. Despite showing a linear behavior of the specimens with copper, the graphs show a noisy behavior. It can also be observed that the sensing range of the composite material with additive is less than with respect to the composite material alone; saturation is faster also with additive (see Figure 30). As the copper content of the compound increases, the sensing range decreases.

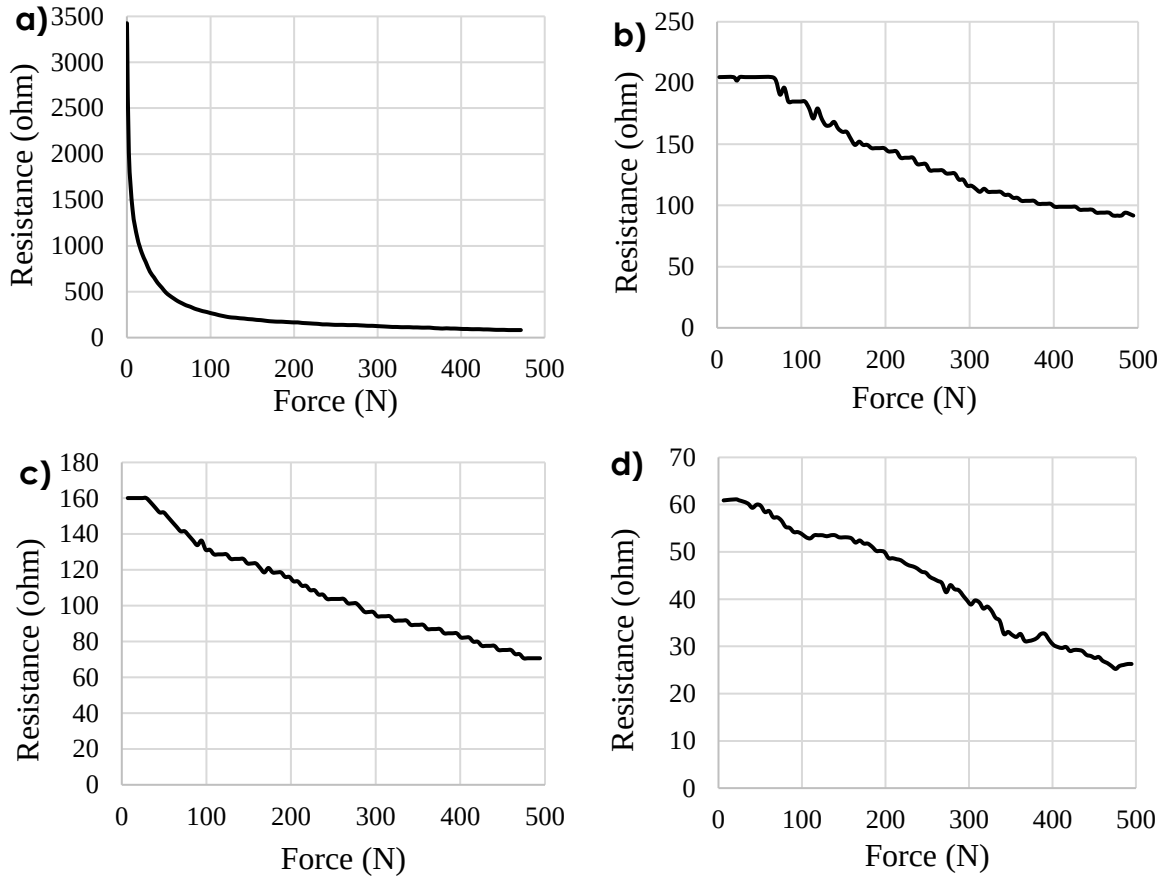

Figure 44. *Resistance vs. Force specimens with copper* ***a)*** *Cu0* ***b)*** *Cu1* ***c)*** *Cu2* ***d)*** *Cu3*

Table 26. *Regression equations of curves*

Specimen	Linear Adjust	R^2	Potential Adjust	R^2
Cu0	R = -2.6212F + 963.68	0.3067	$R = 1932F^{-0.467}$	0.8969
Cu1	R = -0.2583F + 202.8	0.9546	$R = 538.7F^{-0.265}$	0.7799
Cu2	R = -0.1802F + 153.27	0.9744	$R = 422.57F^{-0.264}$	0.8563
Cu3	R = -0.08F + 63.645	0.9825	$R = 184.69F^{-0.281}$	0.7107

Table 27 shows that the sensitivity decreases as the concentration of copper in the compound increases due to its conductive character. The compound has piezoresistive properties, that is, its resistance varies as pressure is exerted. if the electrical resistance of the material decreases, its response is less to the stimulus. It is also to be expected that the conductivity increases as the copper content increases. A decrease in gauge factor is observed as the copper concentration increases, this is due to the decrease in the resistance change of the material as a sensor. The standard deviation of the gauge factor of the samples with copper is 0.05, this means that the sensing capacity of the three samples does not vary significantly.

Table 27. *Characterization as sensor of composite material with copper as additive*

Specimen	wt% CW	Conductivity (S/m)	Sensitivity (Ω/5N)	GF
Cu0	0	0.003	1.55	4.70
Cu1	5	0.004	1.30	3.41
Cu2	10	0.005	0.99	3.29
Cu3	15	0.011	0.56	3.31

Chapter 8

8. Conclusions

8.1. Conclusions

A polymer matrix ceramic particle complex composite fabricated from a conductive polymer resin and a mix of ceramics powders (graphite, ZnO and manganese oxide) obtained from primary battery wastes, has been successfully fabricated in this research. The ceramic powder generated agglomeration in the mix resin-waste. The density between the formulations has no significant differences. With the waste addition, it was found that hardness has a decreasing trend, while that compressive strength has an increasing trend. The piezoresistive effect of the material was verified. The characteristics of the piezoresistive sensor depend on the concentration of the battery residue and the geometry of the electrode. The percolation threshold is nearly to 5 wt% BW.

When copper is used as an additive, there is a linearization of the behavior of the sensor, although it also presents some noise. The gauge factor for copper samples has little variation, but the value is acceptable for applications such as motion detection. Increasing the percentage of copper decreases the sensitivity of the sensor but increases the conductivity.

Because this primary BW is the highest volume of BW in Colombia and in many developing countries, the solution is an alternative to give uses to this waste, and thus, have a positive impact in the environment. Copper is also an element that can be obtained from the recycling of electronic waste, thus contributing to the environment and the development of new electrical materials, closing production cycles. The main issue found in this research was the high contraction of the resin specimens.

The composite material manufactured with and without additives has a potential use in electronic applications as a piezoresistive sensor, which can be used in different fields such as motion detection and thanks to its flexibility, its power can also be studied as a wearable sensor.

Colombia requires strategic solutions in order to give use to BW as most of them are going to landfills, similar to many wastes including hazardous wastes.

8.2. Future work

- Explore dynamic properties of composite material, charge / discharge cycles, and asynchronous studies.
- Determine the effects of temperature on the electrical properties of the material.
- Determine the thermal stability of the composite material with and without additive.

Appendix

Publications in scientific journals

Cardona-Vivas, Natalia, Mauricio A. Correa, and Henry A. Colorado. "Recycling Technologies of Zn–C Batteries: Review and Challenges for a Circular Economy in Colombia." *Energy Technology 2020: Recycling, Carbon Dioxide Management, and Other Technologies*. Springer, Cham, 2020. 377-386.

Publications in other journals

Cardona-Vivas, Natalia. "Huella Ambiental de Mercurio por la Minería de Oro en Colombia." Ingeniería y Sociedad 13 (2018): 8-14.

Participation in scientific events

- CIM 2019 X Congreso Internacional de Materiales. Conference held from October 23 - 25, 2019 in Bucaramanga, Santander, Colombia. Role in the event: Speaker. "Tecnología de Reciclaje de Baterías Zn-C"
- TMS 2020 149th Annual Meeting & Exhibition. Conference held from February 22 - 27, 2020 in San Diego, California, U.S.A. Role in the event: Speaker " Recycling Technologies of Zn–C Batteries: Review and Challenges for a Circular Economy in Colombia " in the symposium "REWAS 2020: Secondary and Byproduct Sources of Materials, Minerals, and Metals".

Membership in international organizations

American Ceramic Society (ACerS). 2019-2020.

References

[1] A. M. Bernardes, D. C. R. Espinosa, and J. A. S. Tenório, "Recycling of batteries: A review of current processes and technologies," *J. Power Sources*, vol. 130, no. 1–2, pp. 291–298, 2004.

[2] D. Linden and T. B. Reddy, *Handbook of batteries*, vol. 33, no. 04. 2013.

[3] European Portable Battery Association, "No," 2014. [Online]. Available: https://www.epba-europe.org/.

[4] GIR (Global Info Research), "Global Zinc-Carbon Battery Market 2019 by Manufacturers, Regions, Type and Application, Forecast to 2024," 2018.

[5] Portafolio, "El mercado de pilas también se energiza en NavidadPortafolio. (2014). El mercado de pilas también se energiza en Navidad. Portafolio.," *Portafolio*, 2014.

[6] REDACCIÓN TECNÓSFERA, "En 2018 los rellenos sanitarios en Colombia recibieron menos pilas," 2019.

[7] Ministerio del Medio Ambiente del Gobierno de Chile, "Diagnóstico producción, importación y distribución y el manejo de los residuos de pilas," 2010.

[8] M. de A. V. y D. Territorial, "Resolucion 1297 de 2010," 2010.

[9] K. Tanong, L. Coudert, G. Mercier, and J. F. Blais, "Recovery of metals from a mixture of various spent batteries by a hydrometallurgical process," *J. Environ. Manage.*, 2016.

[10] I. De Michelis, F. Ferella, E. Karakaya, F. Beolchini, and F. Vegliò, "Recovery of zinc and manganese from alkaline and zinc-carbon spent batteries," *J. Power Sources*, 2007.

[11] H. A. Colorado and S. A. Colorado, "Portland cement with battery waste contents," in *REWAS 2016: Towards Materials Resource*

Sustainability, 2016.

[12] J. Nan, D. Han, M. Cui, M. Yang, and L. Pan, "Recycling spent zinc manganese dioxide batteries through synthesizing Zn-Mn ferrite magnetic materials," *J. Hazard. Mater.*, vol. 133, no. 1–3, pp. 257–261, 2006.

[13] G. Belardi, R. Lavecchia, F. Medici, and L. Piga, "Thermal treatment for recovery of manganese and zinc from zinc-carbon and alkaline spent batteries," *Waste Manag.*, vol. 32, no. 10, pp. 1945–1951, 2012.

[14] E. Sayilgan *et al.*, "A review of technologies for the recovery of metals from spent alkaline and zinc-carbon batteries," *Hydrometallurgy*, vol. 97, no. 3–4, pp. 158–166, 2009.

[15] A. 't Serstevens, "Method for recycling and treating of salt and alkaline batteries," EP1148571B1, 2000.

[16] T. Zenger, A. Krebs, J. Huibert, and H. Van Deutekom, "Method of and apparatus for dismantling and storage of objects comprising alkali metal, such as alkali metal containing batteries," EP1333523B1, 2003.

[17] S. Fröhlich and D. Sewing, "The BATENUS process for recycling mixed battery waste," *J. Power Sources*, 1995.

[18] J. F. Equey, "Recymet: our experience in the recycling of spent batteries," *Proc. Fourth Int. Batter. Recycl. Congr.*, 1998.

[19] H. Jordi, "A financing system for battery recycling in Switzerland," *J. Power Sources*, 1995.

[20] C. J. L. Poinsignon and F. Tedjar, "Method for electrolytical processing of used batteries," EP0620607B1, 1993.

[21] G. Cangini, L. Figari, L. Moglie, and A. Pescetelli, "Process for treating spent batteries," US 5,242,482, 1992.

[22] J. Hanulik, "Process for the recycling of batteries, especially dry batteries," US 6,009,817, 1995.

[23] G. Diaz and D. Andrews, "Placid - A clean process for recycling lead from batteries," *Jom-Journal Miner. Met. Mater. Soc.*, 1996.

[24] T. T. Nguyen, "Process for the simultaneous recovery of manganese dioxide and zinc," US4992149A, 1990.

[25] U. Ducati, "Hydrometallurgical method for recovering metal materials from spent lead-acid storage batteries," US4460442A, 1981.

[26] L. Toro, F. Veglio', F. Beolchini, F. Pagnanelli, M. Zanetti, and G. Furlani, "Process and plant for the treatment of run-down batteries," EP1684369B1, 2004.

[27] D. W. Cawlfield and L. R. Ward, "Integrated process of using chloric acid to separate zinc oxide and manganese oxide," U.S. 5,411,643, 1994.

[28] K. W. Elliott, "Process for battery recycling," U.S. 5,456,992, 1994.

[29] D. Martin, M. A. Garcia, G. Diaz, and J. Falgueras, "A New Zinc Solvent Recovery Application: Spent Domestic Batteries Treatment Plant," *Proc. Int. Solvent Recover. Conf.*, vol. 1, pp. 201–206, 2001.

[30] C. Morales, "Unas 134 millones de pilas no se reciclan cada año en Colombia," 2019. [Online]. Available: https://www.rcnradio.com/estilo-de-vida/medio-ambiente/unas-134-millones-de-pilas-no-se-reciclan-cada-ano-en-colombia. [Accessed: 18-Jul-2020].

[31] M. de C. I. y Turismo, "RESOLUCIÓN 172 DE 2012," Colombia, Resolución 172, 2012.

[32] IDEAM, "Decreto 4741 de 2005.," *Ministerio de Ambiente Vivienda y Desarrollo Territorial,* 2005. .

[33] M. de A. V. y D. Territorial, "Resolución 1297 de 2010," 2010. [Online]. Available: http://www.minambiente.gov.co/images/AsuntosambientalesySectorialyUrbana/pdf/Programa_posconsumo_existente/resolucion_1297_de_2010_pilas.pdf.

[34] E. Del Valle Mora, *La responsabilidad extendida del productor y los programas posconsumo en Colombia*. 2017.

[35] Ministerio de Ambiente Vivienda y Desarrollo Territorial, "NORMATIVIDAD SOBRE RESIDUOS POSCONSUMO RETOS ACTUALES Y FUTUROS," 2016.

[36] Duracell, "USO, MANTENIMIENTO Y RECICLAJE RESPONSABLE DE LAS PILAS," 2010. [Online]. Available: https://www.duracell-la.com/technology/uso-responsable-de-las-pilas-cuidado-y-

desecho/.

[37] A. Autoridad Nacional de Licencias Ambientales, "Auto No. 01156," 2017.

[38] A. Autoridad Nacional de Licencias Ambientales, "Resolución 0308 de 2012," Bogotá, 2012.

[39] A. Autoridad Nacional de Licencias Ambientales, "Resolución 1287 de 2013," Bogotá, 2013.

[40] J. Vera Méndez, "Análisis de los impactos ambientales asociados a la implementación de los planes posconsumo en Colombia Análisis de los impactos ambientales asociados a la implementación de los planes posconsumo en Colombia," *Univ. Nac. Colomb.*, p. 189, 2018.

[41] A. Asociación Nacional de Empresarios de Colombia, "Colombia es pionera en recolección de pilas usadas." [Online]. Available: https://www.pilascolombia.com/assets/images/documentacion/Comunicado_Campana.pdf.

[42] K. S. Bohorquez Guevara, "Corporación Pilas por el Ambiente tiene más de 4.000 puntos para la recolección de pilas," *La República*, 2019.

[43] "Ecotect SAS," 2017. [Online]. Available: http://ecotecsas.com/pilas-y-baterias/.

[44] M. Geoghegan and G. Hadziioannou, "Polymer Electronics," *Polym. Electron.*, 2013.

[45] H. Bagheri, Z. Ayazi, and M. Naderi, "Conductive polymer-based microextraction methods : A review," *Anal. Chim. Acta*, vol. 767, pp. 1–13, 2013.

[46] G. Anantha-Iyengar *et al.*, "Functionalized conjugated polymers for sensing and molecular imprinting applications," *Prog. Polym. Sci.*, vol. 88, pp. 1–129, 2019.

[47] R. A. De Jesus, M. C.; Fu, Y.; Weiss, "Conductive Polymer Blends Prepared," vol. 37, no. 12, 1997.

[48] L. Rupprecht, *Conductive Polymer and Plastics in Industrial Applications*. New York: Plastics Design Library, 1999.

[49] D. D. Ateh, H. A. Navsaria, and P. Vadgama, "Polypyrrole-based

conducting polymers and interactions with biological tissues," *J. R. Soc. Interface*, vol. 3, no. 11, pp. 741–752, 2006.

[50] F. Ahmed, B. S. Lalia, V. Kochkodan, N. Hilal, and R. Hashaikeh, "Electrically conductive polymeric membranes for fouling prevention and detection: A review," *Desalination*, vol. 391, no. 2015, pp. 1–15, 2016.

[51] G. Wallace and G. Spinks, "Conducting polymers - Bridging the bionic interface," *Soft Matter*, vol. 3, no. 6, pp. 665–671, 2007.

[52] R. Balint, N. J. Cassidy, and S. H. Cartmell, "Conductive polymers: Towards a smart biomaterial for tissue engineering," *Acta Biomater.*, vol. 10, no. 6, pp. 2341–2353, 2014.

[53] R. Ravichandran, S. Sundarrajan, J. R. Venugopal, S. Mukherjee, and S. Ramakrishna, "Applications of conducting polymers and their issues in biomedical engineering," *J. R. Soc. Interface*, vol. 7, no. SUPPL. 5, 2010.

[54] G. Shi, M. Rouabhia, Z. Wang, L. H. Dao, and Z. Zhang, "A novel electrically conductive and biodegradable composite made of polypyrrole nanoparticles and polylactide," *Biomaterials*, vol. 25, no. 13, pp. 2477–2488, 2004.

[55] X. Liu, K. J. Gilmore, S. E. Moulton, and G. G. Wallace, "Electrical stimulation promotes nerve cell differentiation on polypyrrole/poly (2-methoxy-5 aniline sulfonic acid) composites," *J. Neural Eng.*, vol. 6, no. 6, 2009.

[56] M. Ahlskog, M. Reghu, T. Noguchi, and T. Ohnishi, "Doping and conductivity studies on poly(p-phenylene vinylene)," *Synth. Met.*, vol. 89, no. 1, pp. 11–15, 2002.

[57] M. M. Ayad, "Optimum reaction conditions for polypyrrole film deposition with some iron(III) compounds," *Polym. Int.*, 1994.

[58] J. Duchet, R. Legras, and S. Demoustier-Champagne, "Chemical synthesis of polypyrrole: Structure-properties relationship," *Synth. Met.*, vol. 98, no. 2, pp. 113–122, 1998.

[59] G. Inzelt, M. Pineri, J. W. Schultze, and M. A. Vorotyntsev, "Electron and proton conducting polymers: Recent developments and prospects," *Electrochimica Acta*. 2000.

[60] D. Kumar and R. C. Sharma, "Advances in conductive polymers," *Eur.*

Polym. J., vol. 34, no. 8, pp. 1053–1060, 1998.

[61] H. S. Nalwa, *Handbook of Advances Electronic and Photonic Materials and Devices*. Academic Press, 1998.

[62] C. Zhan, G. Yu, Y. Lu, L. Wang, E. Wujcik, and S. Wei, "Conductive polymer nanocomposites: a critical review of modern advanced devices," *J. Mater. Chem. C*, vol. 5, no. 7, pp. 1569–1585, 2017.

[63] S. Belhousse *et al.*, "Functionalization of silicon nanowires by conductive and non-conductive polymers," *Appl. Surf. Sci.*, vol. 421, pp. 134–141, 2017.

[64] N. Kurra, M. K. Hota, and H. N. Alshareef, "Conducting polymer micro-supercapacitors for flexible energy storage and Ac line-filtering," *Nano Energy*, pp. 500–508, 2015.

[65] M. Bharti, A. Singh, S. Samanta, and D. K. Aswal, "Conductive polymers for thermoelectric power generation," *Prog. Mater. Sci.*, vol. 93, pp. 270–310, 2018.

[66] H. C. Soyleyici, "Electrochromic properties of multifunctional conductive polymer based on naphtalene," *Opt. Mater. (Amst).*, pp. 208–214, 2019.

[67] J. William D. Callister, *Materials Science and Engineering 7th Ed. : An Introduction*. 2007.

[68] R. D. Matthews, Frank L and Rawlings, *Composite materials: engineering and science*. CRC press, 1999.

[69] R.-M. Wang, S.-R. Zheng, and Y.-P. Zheng, "Introduction to polymer matrix composites," in *Polymer Matrix Composites and Technology*, 2011.

[70] H. Shirakawa and S. Ikeda, "Infrared spectra of poly(acetylene)," *Polym. J.*, 2002.

[71] D. Jang, H. N. Yoon, I. W. Nam, and H. K. Lee, "Effect of carbonyl iron powder incorporation on the piezoresistive sensing characteristics of CNT-based polymeric sensor," *Compos. Struct.*, 2020.

[72] G. Shi *et al.*, "Highly Sensitive, Wearable, Durable Strain Sensors and Stretchable Conductors Using Graphene/Silicon Rubber Composites," *Adv. Funct. Mater.*, 2016.

[73] M. Zhang, C. Wang, H. Wang, M. Jian, X. Hao, and Y. Zhang, "Carbonized Cotton Fabric for High-Performance Wearable Strain Sensors," *Adv. Funct. Mater.*, 2017.

[74] M. Amjadi, A. Pichitpajongkit, S. Lee, S. Ryu, and I. Park, "Highly stretchable and sensitive strain sensor based on silver nanowire-elastomer nanocomposite," *ACS Nano*, 2014.

[75] J. J. Park, W. J. Hyun, S. C. Mun, Y. T. Park, and O. O. Park, "Highly stretchable and wearable graphene strain sensors with controllable sensitivity for human motion monitoring," *ACS Appl. Mater. Interfaces*, 2015.

[76] H. Mahandra, R. Singh, and B. Gupta, "Recycling of Zn-C and Ni-Cd spent batteries using Cyphos IL 104 via hydrometallurgical route," *J. Clean. Prod.*, 2018.

[77] B. Ebin, M. Petranikova, B. M. Steenari, and C. Ekberg, "Production of zinc and manganese oxide particles by pyrolysis of alkaline and Zn-C battery waste," *Waste Manag.*, 2016.

[78] S. Abid Charef, A. M. Affoune, A. Caballero, M. Cruz-Yusta, and J. Morales, "Simultaneous recovery of Zn and Mn from used batteries in acidic and alkaline mediums: A comparative study," *Waste Manag.*, 2017.

[79] D. Rahangdale and A. Kumar, "Acrylamide grafted chitosan based ion imprinted polymer for the recovery of cadmium from nickel-cadmium battery waste," *J. Environ. Chem. Eng.*, 2018.

[80] F. Rahmawati, L. Yuliati, I. S. Alaih, and F. R. Putri, "Carbon rod of zinc-carbon primary battery waste as a substrate for CdS and TiO2photocatalyst layer for visible light driven photocatalytic hydrogen production," *Journal of Environmental Chemical Engineering*, vol. 5, no. 3. pp. 2251–2258, 2017.

[81] H. Huang *et al.*, "Converting spent battery anode waste into a porous biocomposite with high Pb(II) ion capture capacity from solution," *Journal of Cleaner Production*, vol. 184. pp. 622–631, 2018.

[82] C. W. Liu, C. H. Lin, and Y. P. Fu, "Mn-Zn ferrite powder preparation by hydrothermal process from used dry batteries," *Japanese J. Appl. Physics, Part 1 Regul. Pap. Short Notes Rev. Pap.*, vol. 45, no. 5 A, pp. 4040–4041, 2006.

[83] M. V. Gallegos, M. A. Peluso, E. Finocchio, H. J. Thomas, G. Busca, and J. E. Sambeth, "Removal of VOCs by catalytic process. A study of MnZnO composites synthesized from waste alkaline and Zn/C batteries," *Chem. Eng. J.*, vol. 313, pp. 1099–1111, 2017.

[84] T. Dutta *et al.*, "Recovery of nanomaterials from battery and electronic wastes: A new paradigm of environmental waste management," *Renew. Sustain. Energy Rev.*, vol. 82, no. March 2017, pp. 3694–3704, 2018.

[85] L. El Fissi *et al.*, "OSTEMER polymer as a rapid packaging of electronics and microfluidic system on PCB," *Sensors Actuators A Phys.*, vol. 8, no. 5, p. 55, 2019.

[86] P. F. Flowers, C. Reyes, S. Ye, M. J. Kim, and B. J. Wiley, "3D printing electronic components and circuits with conductive thermoplastic filament," *Addit. Manuf.*, vol. 18, pp. 156–163, 2017.

[87] J. R. Dios, C. Garcia-Astrain, S. Gonçalves, P. Costa, and S. Lanceros-Méndez, "Piezoresistive performance of polymer-based materials as a function of the matrix and nanofiller content to walking detection application," *Compos. Sci. Technol.*, 2019.

[88] A. Ferreira, M. T. Martínez, A. Ansón-Casaos, L. E. Gómez-Pineda, F. Vaz, and S. Lanceros-Mendez, "Relationship between electromechanical response and percolation threshold in carbon nanotube/poly(vinylidene fluoride) composites," *Carbon N. Y.*, 2013.

[89] F. Avilés, A. May-Pat, M. A. López-Manchado, R. Verdejo, A. Bachmatiuk, and M. H. Rümmeli, "A comparative study on the mechanical, electrical and piezoresistive properties of polymer composites using carbon nanostructures of different topology," *Eur. Polym. J.*, 2018.

[90] S. Gong, Z. H. Zhu, and S. A. Meguid, "Carbon nanotube agglomeration effect on piezoresistivity of polymer nanocomposites," *Polymer (Guildf).*, 2014.

[91] M. Chaturvedi, V. Panwar, and B. Prasad, "Piezoresistive sensitivity tuning using polyelectrolyte as interface linker in carbon based polymer composites," *Sensors Actuators, A Phys.*, 2020.

[92] L. Duan *et al.*, "Designing formulation variables of extrusion-based manufacturing of carbon black conductive polymer composites for piezoresistive sensing," *Compos. Sci. Technol.*, 2019.

[93] P. Zhang *et al.*, "The effects of agglomerate on the piezoresistivity of conductive carbon nanotube/polyvinylidene fluoride composites," *Sensors Actuators, A Phys.*, 2018.

[94] W. Zhai *et al.*, "Multifunctional flexible carbon black/polydimethylsiloxane piezoresistive sensor with ultrahigh linear range, excellent durability and oil/water separation capability," *Chem. Eng. J.*, 2019.

[95] J. Wang, B. Tian, Z. Niu, S. Qi, Y. Bao, and B. Xin, "Synthesis of nano-sized Zn–Mn ferrite from the resulting bioleachate of obsolete Zn–Mn batteries at a high pulp density of 5.0% enhanced by the added Fe3+," *J. Clean. Prod.*, vol. 229, pp. 299–307, 2019.

[96] R. Farzana, R. Rajarao, K. Hassan, P. R. Behera, and V. Sahajwalla, "Thermal nanosizing: Novel route to synthesize manganese oxide and zinc oxide nanoparticles simultaneously from spent Zn–C battery," *J. Clean. Prod.*, vol. 196, pp. 478–488, 2018.

[97] "Introduction Chemical structure Physical."

[98] H. Villasenor-Ochoa, "Engineering fundamentals refresh : Strength vs stiffness vs hardness," 2017. [Online]. Available: http://www.fictiv.com/hwg/design/engineering-fundamentals-refresh-strength-vs-stiffness-hardness.

[99] A. D. Loaeza Becerril, "Obtención de curvas esfuerzo-deformación verdaderas del PP y copolímeros en bloque a velocidad de deformación constante aplicando correlación de imágenes digitales," Universitat Politècnica de Catalunya, 2014.

[100] FSR, "Force Sensing Resistor. Integration Guide and Evaluation Parts Catalogue. Interlink Electronics."

[101] D. A. Valle-Lopera, A. F. Castaño-Franco, J. Gallego-Londoño, and A. M. Hernández-Valdivieso, "Test and fabrication of piezoresistive sensors for contact pressure measurement," *Rev. Fac. Ing.*, vol. 2017, no. 82, pp. 47–52, 2017.

[102] P. Costa, J. Silva, V. Sencadas, R. Simoes, J. C. Viana, and S. Lanceros-Méndez, "Mechanical, electrical and electro-mechanical properties of thermoplastic elastomer styrene-butadiene-styrene/multiwall carbon nanotubes composites," *J. Mater. Sci.*, 2013.

[103] S. Kirkpatrick, "Percolation and Conduction," *Rev. Mod. Phys.*, 1973.

[104] M. Grujicic, G. Cao, and W. N. Roy, "A computational analysis of the percolation threshold and the electrical conductivity of carbon nanotubes filled polymeric materials," *J. Mater. Sci.*, 2004.

[105] L. Chang, K. Friedrich, L. Ye, and P. Toro, "Evaluation and visualization of the percolating networks in multi-wall carbon nanotube/epoxy composites," *J. Mater. Sci.*, 2009.

[106] S. Wang *et al.*, "Theoretical modeling and experimental verification of percolation threshold with MWCNTs' rotation and translation around a growing bubble in conductive polymer composite foams," *Compos. Sci. Technol.*, vol. 199, no. June, p. 108345, 2020.

[107] W. E. Mahmoud, M. H. I. El-Eraki, A. M. Y. El-Lawindy, and H. H. Hassan, "The mechanical behaviour of NBR/FEF under compressive cyclic stress-strain," *J. Phys. D. Appl. Phys.*, 2006.

[108] W. Wersing, "Ferroelectric Devices," in *Ferroelectric Ceramics*, 1993.

[109] N. Abdel-Aal, F. El-Tantawy, A. Al-Hajry, and M. Bououdina, "Epoxy resin/plasticized carbon black composites. part I. Electrical and thermal properties and their applications," *Polym. Compos.*, 2008.

[110] Z. Todorova, N. Dishovsky, R. Dimitrov, and F. El-Tantawy, "Investigation of electrical properties of elastomer composites filled with TiB2," *J. Elastomers Plast.*, 2007.

[111] V. Koncar, "Structural health monitoring of processes related to composite manufacturing," in *Smart Textiles for In Situ Monitoring of Composites*, 2019.

[112] K. A. Dubey, R. K. Mondal, V. Grover, Y. K. Bhardwaj, and A. K. Tyagi, "Development of a novel strain sensor based on fluorocarbon-elastomeric nanocomposites: Effect of network density on the electromechanical properties," *Sensors Actuators, A Phys.*, 2015.

[113] P. Costa, M. F. Carvalho, V. Correia, J. C. Viana, and S. Lanceros-Mendez, "Polymer Nanocomposite-Based Strain Sensors with Tailored Processability and Improved Device Integration," *ACS Appl. Nano Mater.*, 2018.

[114] M. Zheng *et al.*, "Strain sensors based on chromium nanoparticle arrays," *Nanoscale*, 2014.

[115] P. Costa *et al.*, "High-performance graphene-based carbon

nanofiller/polymer composites for piezoresistive sensor applications," *Compos. Sci. Technol.*, 2017.

[116] R. K. Srivastava *et al.*, "The strain sensing and thermal-mechanical behavior of flexible multi-walled carbon nanotube/polystyrene composite films," *Carbon N. Y.*, 2011.

[117] W. Li *et al.*, "Flexible strain sensor based on aerogel-spun carbon nanotube yarn with a core-sheath structure," *Compos. Part A Appl. Sci. Manuf.*, 2018.

[118] T. Yamada *et al.*, "A stretchable carbon nanotube strain sensor for human-motion detection," *Nat. Nanotechnol.*, 2011.

[119] N. D. Alexopoulos, C. Jaillet, C. Zakri, P. Poulin, and S. K. Kourkoulis, "Improved strain sensing performance of glass fiber polymer composites with embedded pre-stretched polyvinyl alcohol-carbon nanotube fibers," *Carbon N. Y.*, 2013.

[120] S. Makireddi, S. Shivaprasad, G. Kosuri, F. V. Varghese, and K. Balasubramaniam, "Electro-elastic and piezoresistive behavior of flexible MWCNT/PMMA nanocomposite films prepared by solvent casting method for structural health monitoring applications," *Compos. Sci. Technol.*, 2015.

[121] M. Pavlin and F. Novak, "Yield enhancement of piezoresistive pressure sensors for automotive applications," *Sensors Actuators, A Phys.*, 2008.

[122] F. Hartmann, "Semiconductor sensors," in *Nuclear Instruments and Methods in Physics Research, Section A: Accelerators, Spectrometers, Detectors and Associated Equipment*, 2011.

[123] A. Hernández, L. E. Farah, J. Ramírez, and E. Charry, "New thermal compensation algorithm for piezoresistive pressure sensors based on the linear approximation by segments," *Métodos numéricos para cálculo y diseño en Ing. Rev. Int.*, 2015.